Cross section measurement of $e^+e^- \to \Lambda_c^+\bar{\Lambda}_c^-$ near threshold at BESIII

Weiping Wang [1], Weimin Song [2], Xiaorong Zhou [1],
Liang Yan [1], Ronggang Ping [2], Guangshun Huang [1], Changzheng Yuan [2],
Kai Zhu [2], R. Baldini Ferroli [3], Zhengguo Zhao [1]

[1] University of Science and Technology of China, Anhui, China
[2] Institute of High Energy Physics, CAS, Beijing, China
[3] INFN, Laboratori Nazionali di Frascati, Frascati, Italy

Abstract

We study the process of $e^+e^- \to \Lambda_c^+\bar{\Lambda}_c^-$ at center-of-mass energies($\sqrt{s}$) of 4.574, 4.580, 4.590 and 4.599 GeV with the data sample collected with BESIII detector at BEPCII. The energy dependence of the cross section of $e^+e^- \to \Lambda_c^+\bar{\Lambda}_c^-$ is measured in two ways: by reconstructing Λ_c^+ with the golden mode $\Lambda_c^+ \to p^+K^-\pi^+$ and by reconstructing Λ_c^+ with the multiple decay modes. The $\bar{\Lambda}_c^-$ is reconstructed independently and the Born cross section is obtained from the weighted average of that obtained from tagging Λ_c^+ and tagging $\bar{\Lambda}_c^-$. The very weak energy dependence of the cross section near threshold indicates that the traditional theoretical prediction, which did not take account the strong interaction, needs to be modified. With the large statistic of multiple decay modes, we estimate the $|G_E/G_M|$ ratio to be 1.47 ± 0.22 at $\sqrt{s} = 4.574$ GeV and 1.23 ± 0.06 at $\sqrt{s} = 4.599$ GeV by fitting the angular distribution of Λ_c^+ and $\bar{\Lambda}_c^-$. By assuming a uniform magnetic form factor ($|G_M|$) near threshold, a fit is performed on the cross section line-shape and the form factor $|G_M|$ is yield to be 1.073 ± 0.022 near threshold.

PACS numbers: 14.40.Pq, 13.25.Gv, 13.40.Hq

CONTENTS

I. INTRODUCTION

Get blank!!

II. CROSS SECTION MEASUREMENT OF $e^+e^- \to \Lambda_c^+\bar{\Lambda}_c^-$ BY TAGGING MULTIPLE DECAY MODES

A. Decay modes and event selection

TABLE I. The tagged decay modes of Λ_c^+ in this analysis.

Decay modes	Intermediate BR	Absolute BR(%)	Total BR(%)
1. $\Lambda_c^+ \to p^+K^-\pi^+$	–	5.64 ± 0.35	5.64 ± 0.35
2. $\Lambda_c^+ \to p^+K_S^0$, $K_S^0 \to \pi^+\pi^-$	69.2%	1.47 ± 0.09	1.02 ± 0.06
3. $\Lambda_c^+ \to \Lambda\pi^+$, $\Lambda \to p^+\pi^-$	63.9%	1.19 ± 0.08	0.76 ± 0.05
4. $\Lambda_c^+ \to p^+K^-\pi^+\pi^0$, $\pi^0 \to \gamma\gamma$	98.8%	4.22 ± 0.36	4.17 ± 0.36
5. $\Lambda_c^+ \to p^+K_S^0\pi^0$, $K_S^0 \to \pi^+\pi^-$, $\pi^0 \to \gamma\gamma$	69.2%×98.8%	1.75 ± 0.13	1.20 ± 0.09
6. $\Lambda_c^+ \to \Lambda\pi^+\pi^0$, $\Lambda \to p^+\pi^-$, $\pi^0 \to \gamma\gamma$	63.9%×98.8%	6.67 ± 0.40	4.21 ± 0.25
7. $\Lambda_c^+ \to p^+K_S^0\pi^+\pi^-$, $K_S^0 \to \pi^+\pi^-$	69.2%	1.46 ± 0.13	1.01 ± 0.09
8. $\Lambda_c^+ \to \Lambda\pi^+\pi^+\pi^-$, $\Lambda \to p^+\pi^-$	63.9%	3.66 ± 0.27	2.34 ± 0.17
9. $\Lambda_c^+ \to \Sigma^0\pi^+$, $\Sigma^0 \to \Lambda\gamma$, $\Lambda \to p^+\pi^-$	63.9%	1.21 ± 0.08	0.77 ± 0.05
10.$\Lambda_c^+ \to \Sigma^+\pi^+\pi^-$, $\Sigma^+ \to p\pi^0$, $\pi^0 \to \gamma\gamma$	51.6%×98.8%	4.05 ± 0.30	2.06 ± 0.15

TABLE II. The resolution of ΔE for each mode and the resolution of the intermediate state invariant mass at $\sqrt{s}$ = 4.6 in MeV.

Mode	ΔE requirement(GeV)	Intermediate state	requirement(GeV)
$pK^-\pi^+$	(-0.02,0.02)	$--$	$--$
pK_S^0	(-0.02,0.02)	K_s^0	(0.487,0.511)
$\Lambda\pi^+$	(-0.02,0.02)	Λ	(1.111,1.121)
$pK^-\pi^+\pi^0$	(-0.03,0.02)	π^0	(0.115,0.150)
$pK_S^0\pi^0$	(-0.03,0.02)	K_s^0,π^0	(0.487,0.511),(0.115,0.150)
$\Lambda\pi^+\pi^0$	(-0.03,0.02)	Λ,π^0	(1.111,1.121),(0.115,0.150)
$pK_S^0\pi^+\pi^-$	(-0.02,0.02)	K_s^0	(0.487,0.511)
$\Lambda\pi^+\pi^+\pi^-$	(-0.02,0.02)	Λ	(1.111,1.121)
$\Sigma^0\pi^+$	(-0.02,0.02)	Σ^0,Λ	(1.179,1.203),(1.111,1.121)
$\Sigma^+\pi^+\pi^-$	(-0.03,0.02)	Σ^+,π^0	(1.176,1.200),(0.115,0.150)

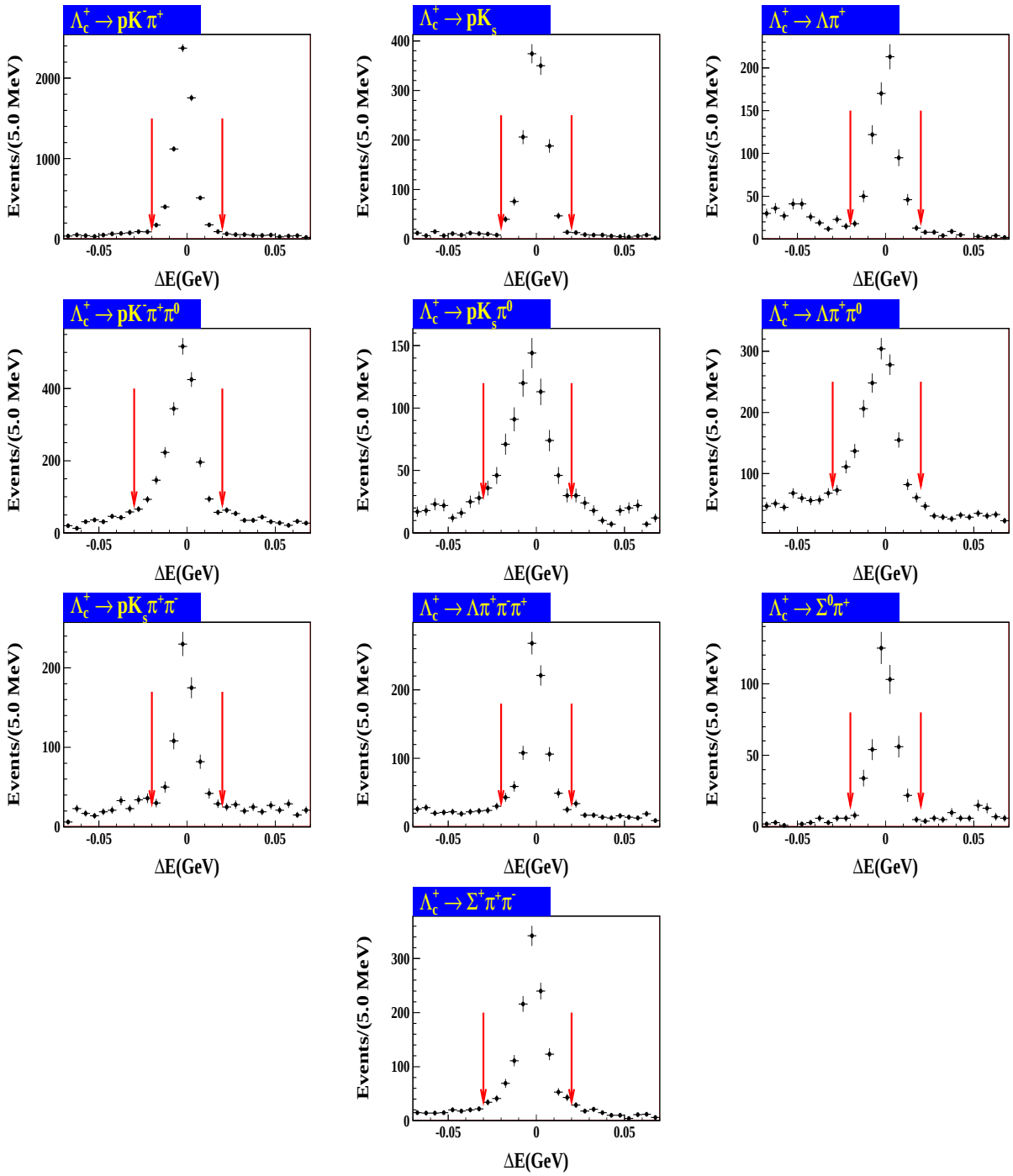

FIG. 1. The distribution of ΔE of each mode at $\sqrt{s} = 4.599$ GeV, where the red arrows indicate the signal region.

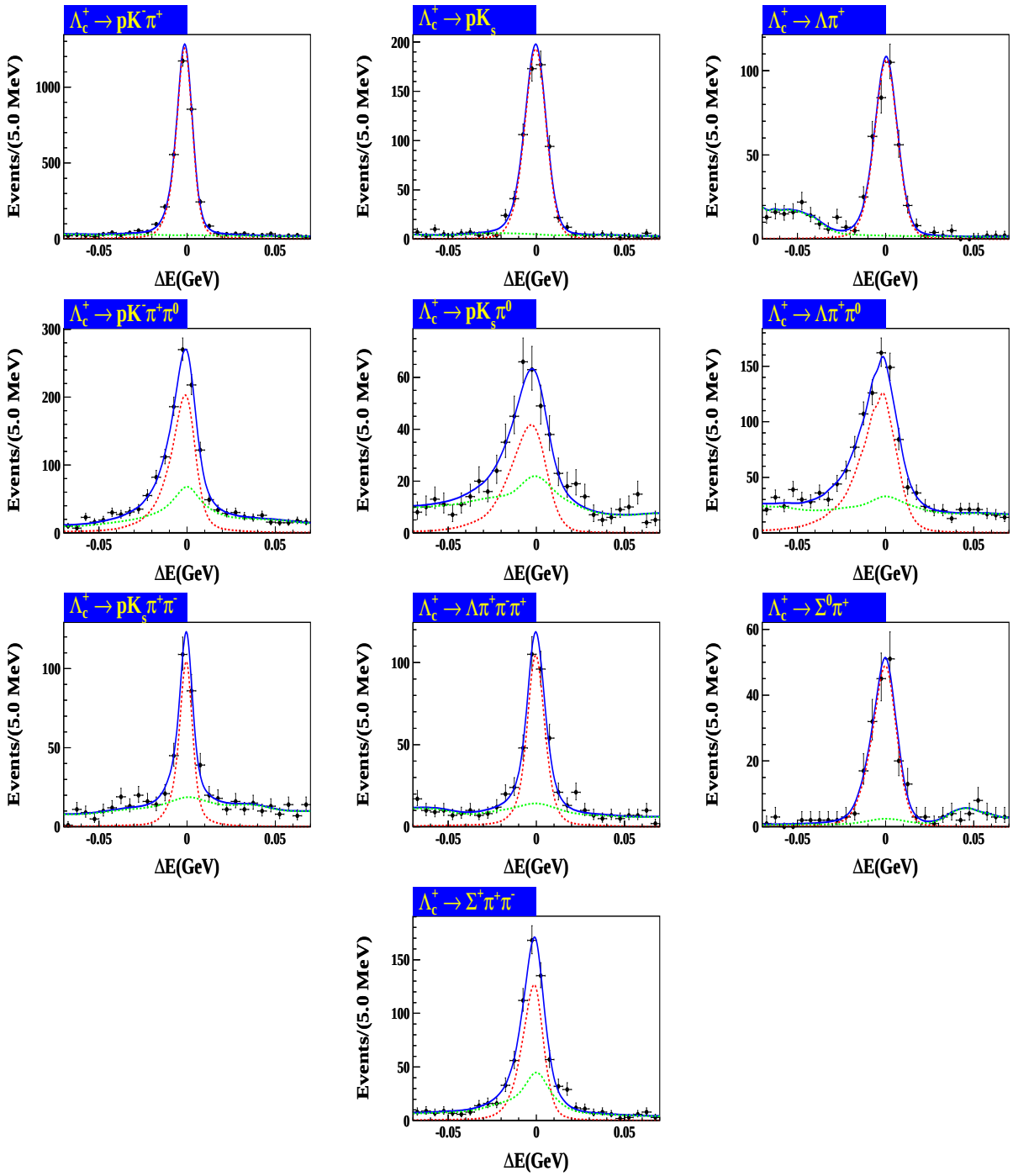

FIG. 2. The distribution of ΔE of each mode at $\sqrt{s}$ = 4.599 GeV, where the red arrows indicate the signal region.

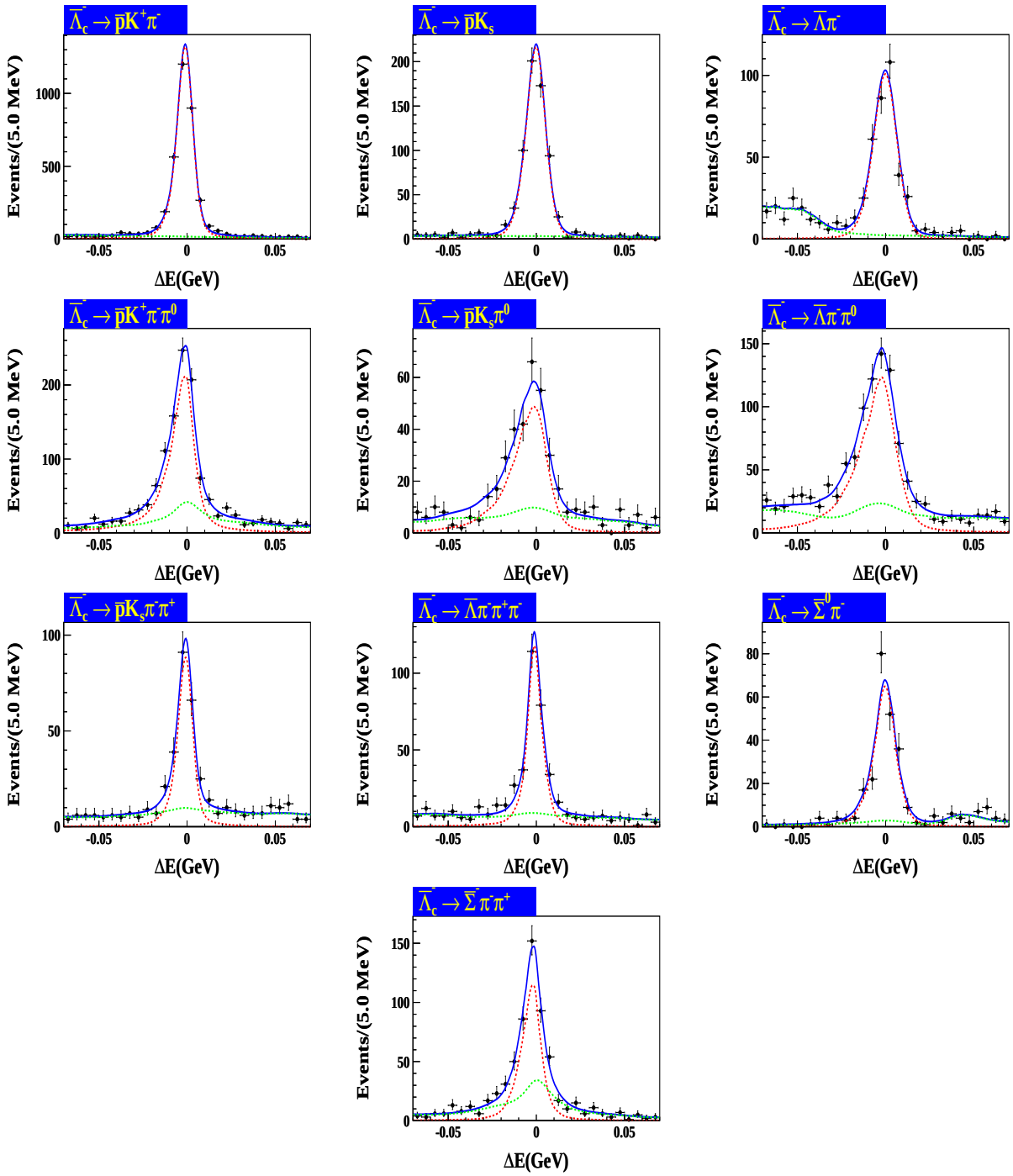

FIG. 3. The distribution of ΔE of each mode at $\sqrt{s}$ = 4.599 GeV, where the red arrows indicate the signal region.

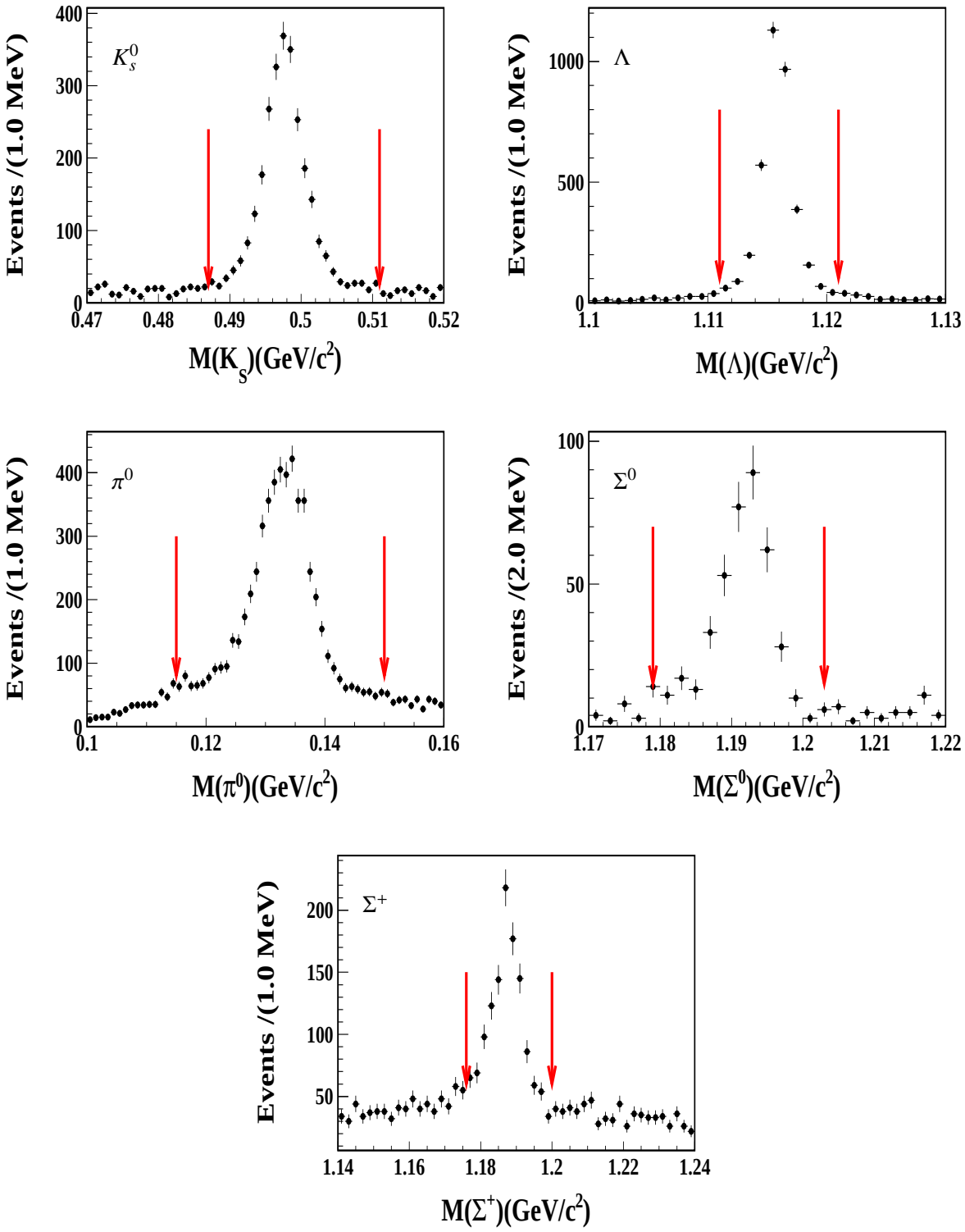

FIG. 4. The invariant mass distribution of intermediated states, where the red arrows indicate the signal region.

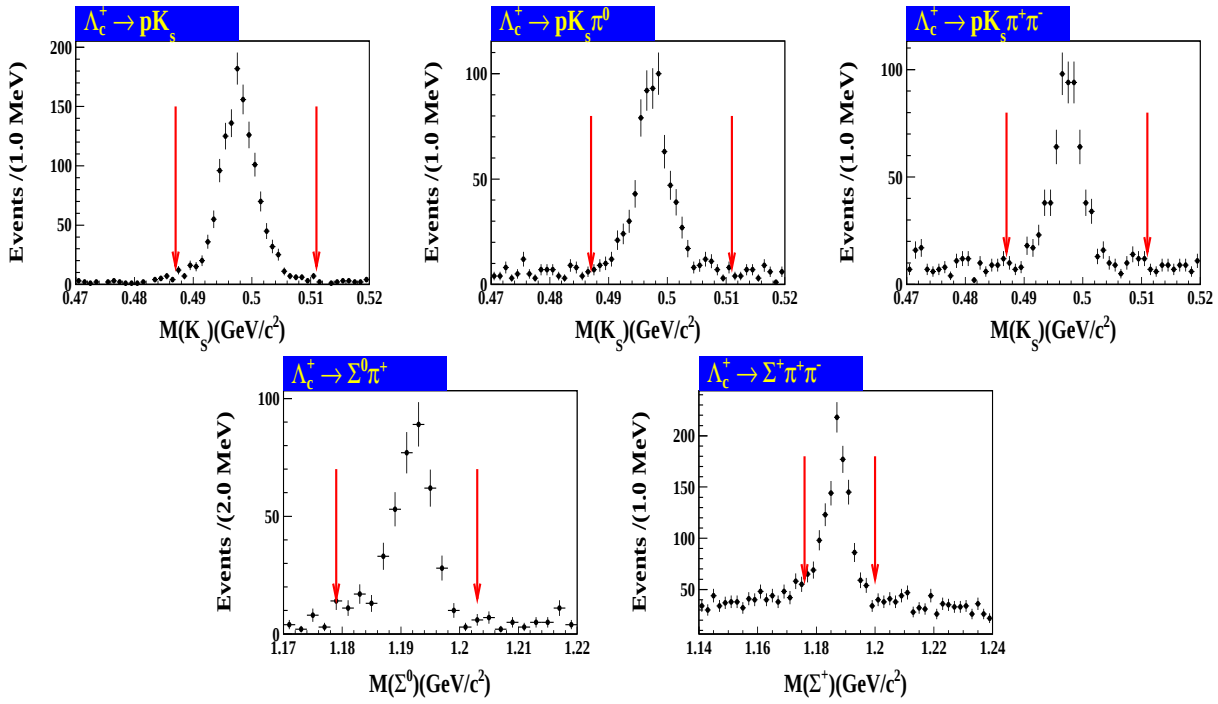

FIG. 5. The invariant mass distribution of intermediated states, where the red arrows indicate the signal region.

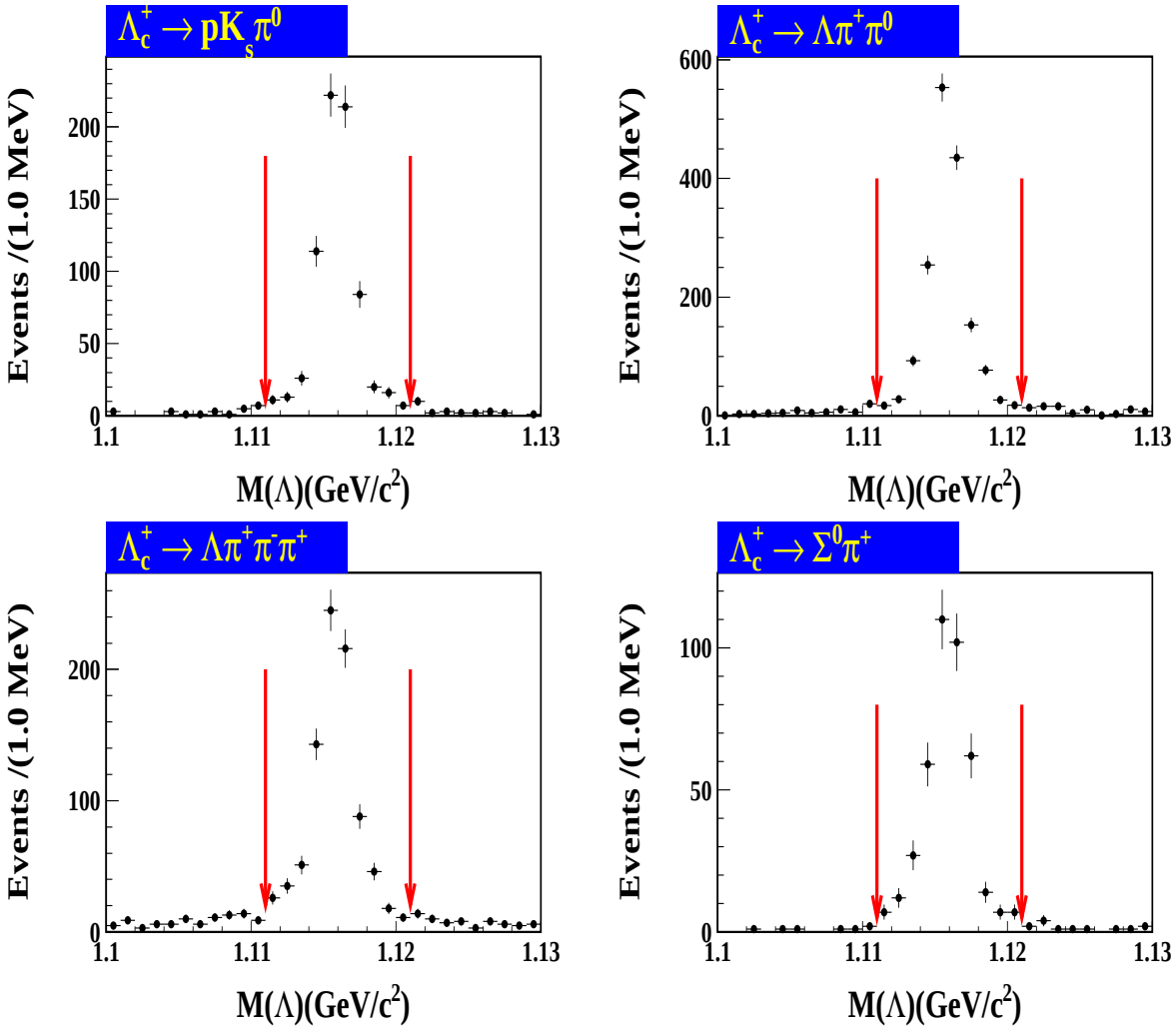

FIG. 6. The invariant mass distribution of intermediated states, where the red arrows indicate the signal region.

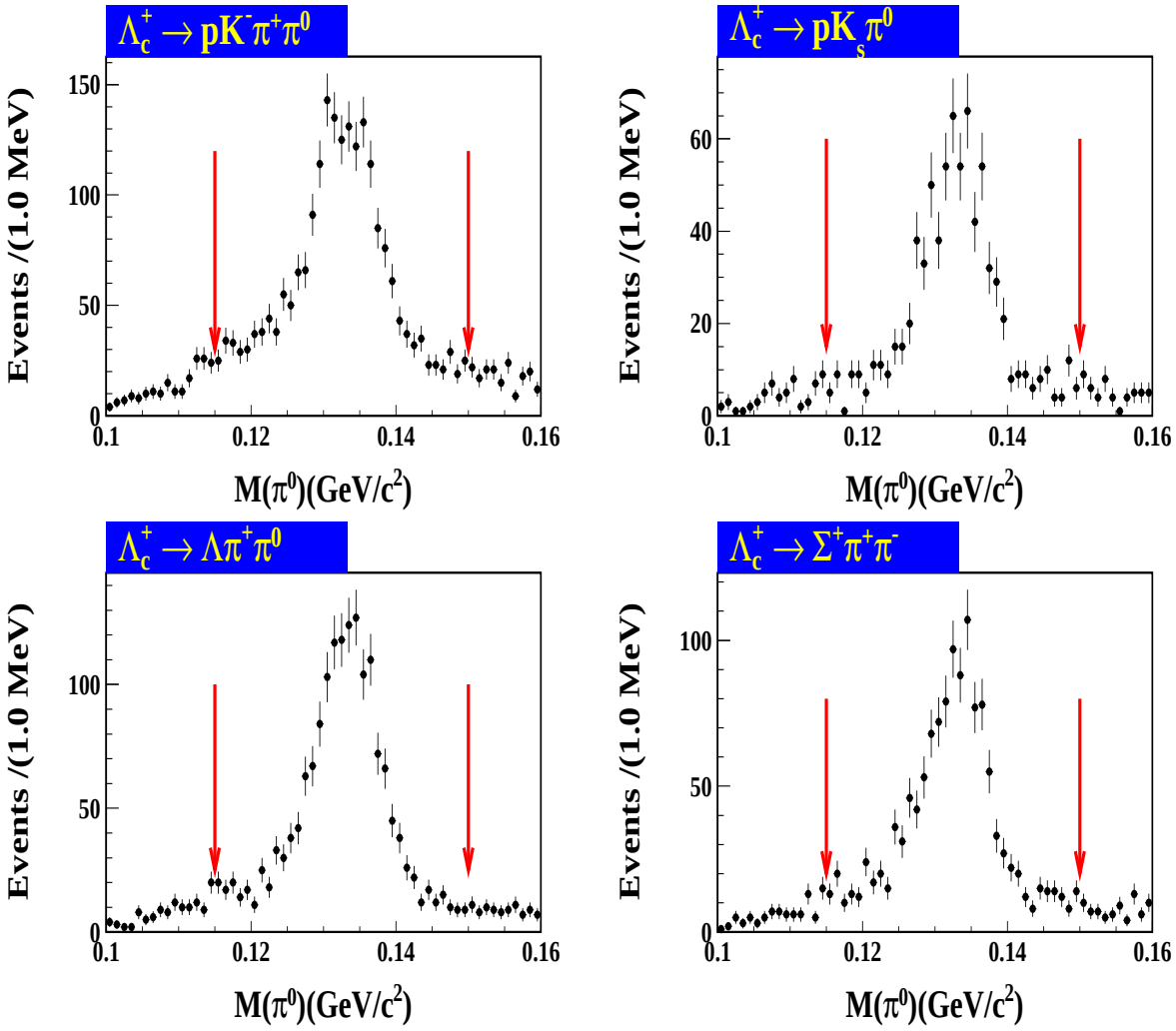

FIG. 7. The invariant mass distribution of intermediated states, where the red arrows indicate the signal region.

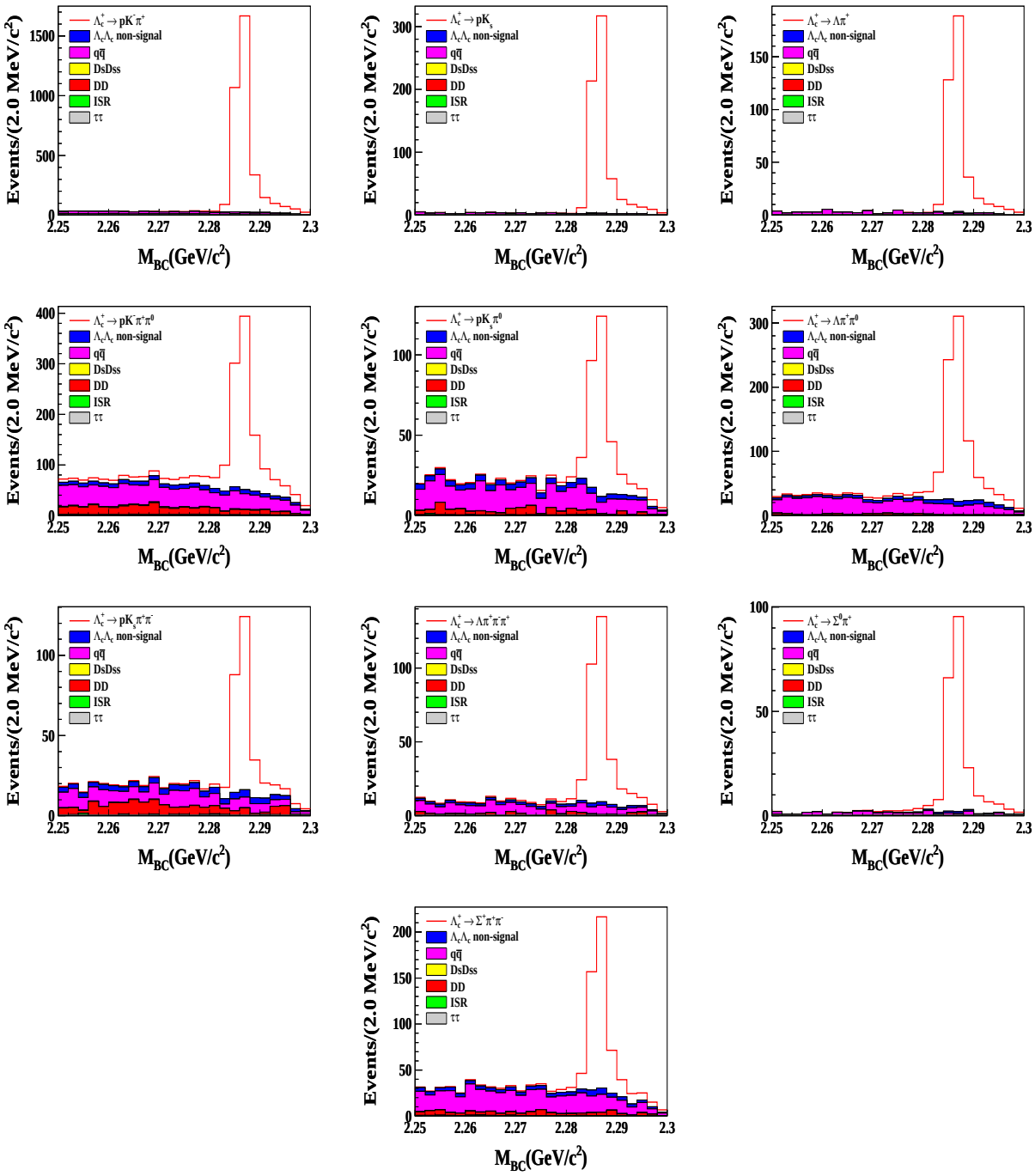

FIG. 8. The distribution of cocktail MC in each mode.

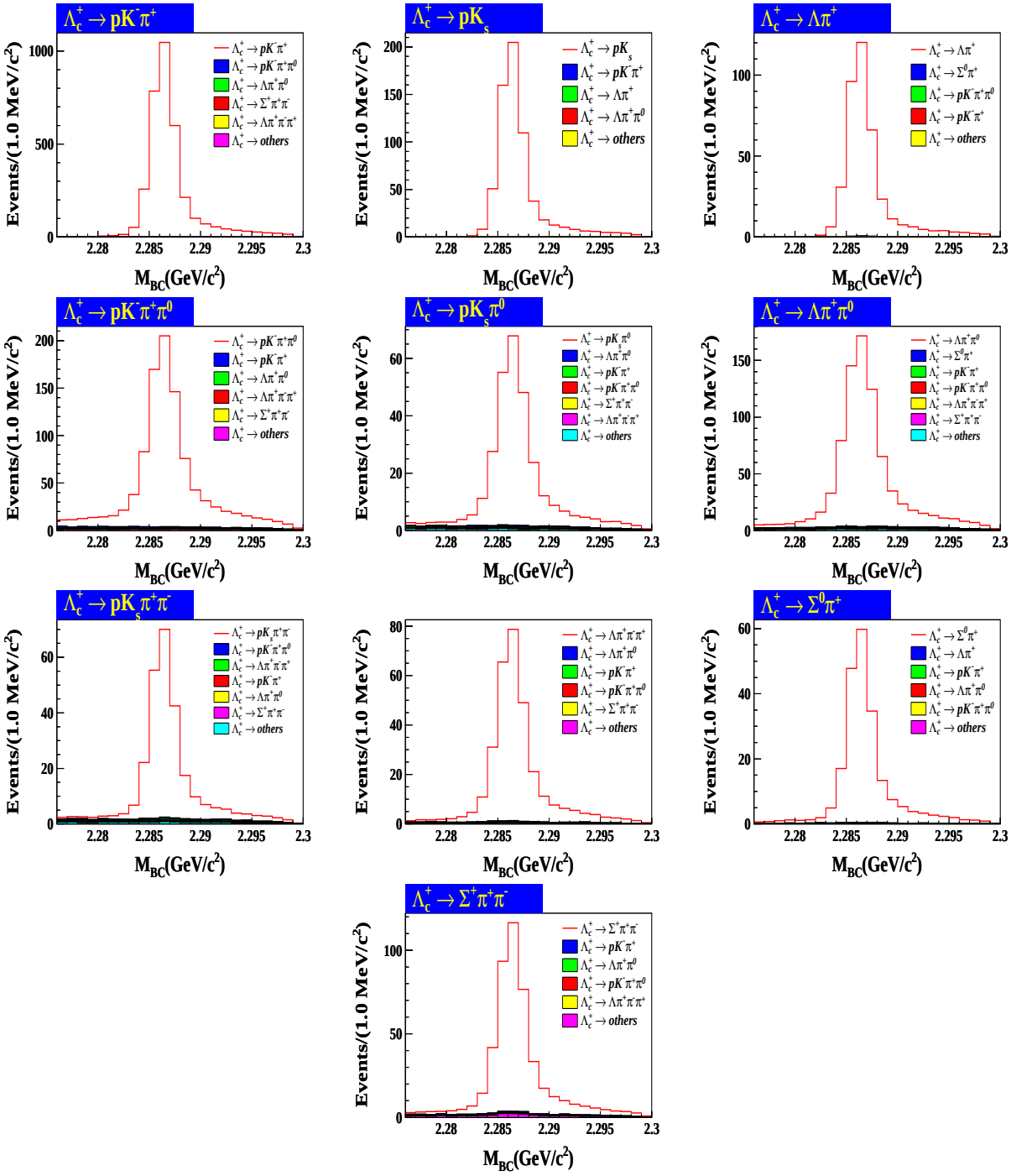

FIG. 9. The distribution of background and signal of MC in signal range for each mode.

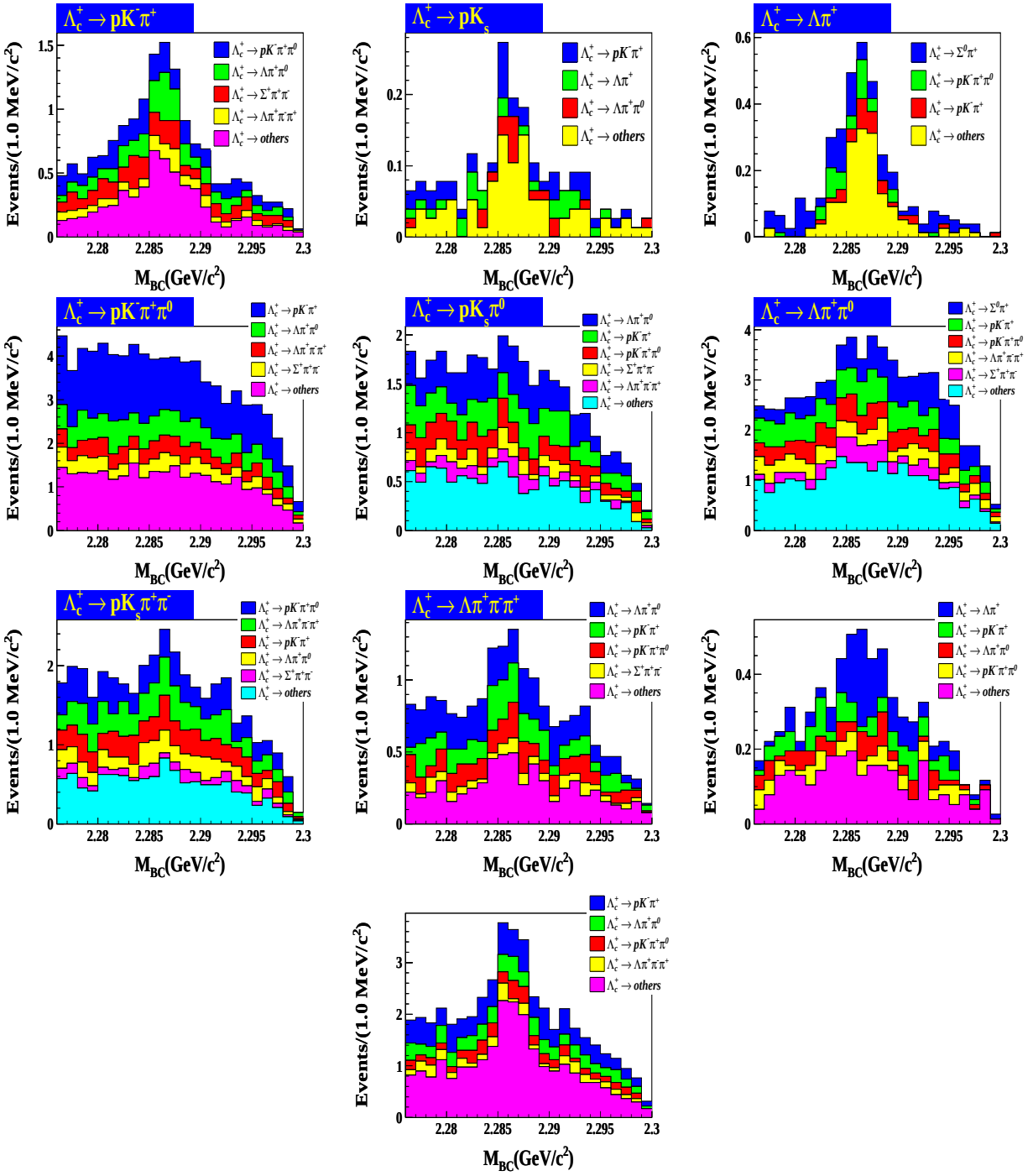

FIG. 10. The distribution of non-signal background of MC in signal range for each mode.

TABLE III. The cross feed yields of each mode at $\sqrt{s}$ = 4.600. We list in percent.

Modes	$pK^-\pi^+$	pK^0_S	$\Lambda\pi^+$	$pK^-\pi^+\pi^0$	$pK^0_S\pi^0$	$\Lambda\pi^+\pi^0$	$pK^0_S\pi^+\pi^-$	$\Lambda\pi^+\pi^+\pi^-$	$\Sigma^0\pi^+$	$\Sigma^+\pi^+\pi^-$
$pK^-\pi^+$	−−	0.0	0.0	0.1	0.0	0.1	0.0	0.0	0.0	0.0
pK^0_S	0.1	−−	0.0	0.0	0.0	0.0	0.0	0.0	0.0	0.0
$\Lambda\pi^+$	0.1	0.0	−−	0.1	0.0	0.1	0.0	0.0	0.3	0.0
$pK^-\pi^+\pi^0$	2.8	0.2	0.2	−−	0.4	1.2	0.3	0.8	0.2	0.6
$pK^0_S\pi^0$	2.0	0.2	0.2	1.4	−−	2.3	0.6	0.7	0.2	0.8
$\Lambda\pi^+\pi^0$	1.3	0.2	0.2	1.0	0.4	−−	0.2	0.8	1.4	0.6
$pK^0_S\pi^+\pi^-$	2.2	0.3	0.3	2.6	1.0	1.6	−−	2.5	0.2	0.8
$\Lambda\pi^+\pi^+\pi^-$	1.1	0.2	0.1	0.9	0.2	1.5	0.3	−−	0.1	0.4
$\Sigma^0\pi^+$	0.4	0.1	0.7	0.3	0.1	0.4	0.1	0.1	−−	0.2
$\Sigma^+\pi^+\pi^-$	2.0	0.2	0.1	0.8	0.4	1.3	0.2	0.7	0.1	−−

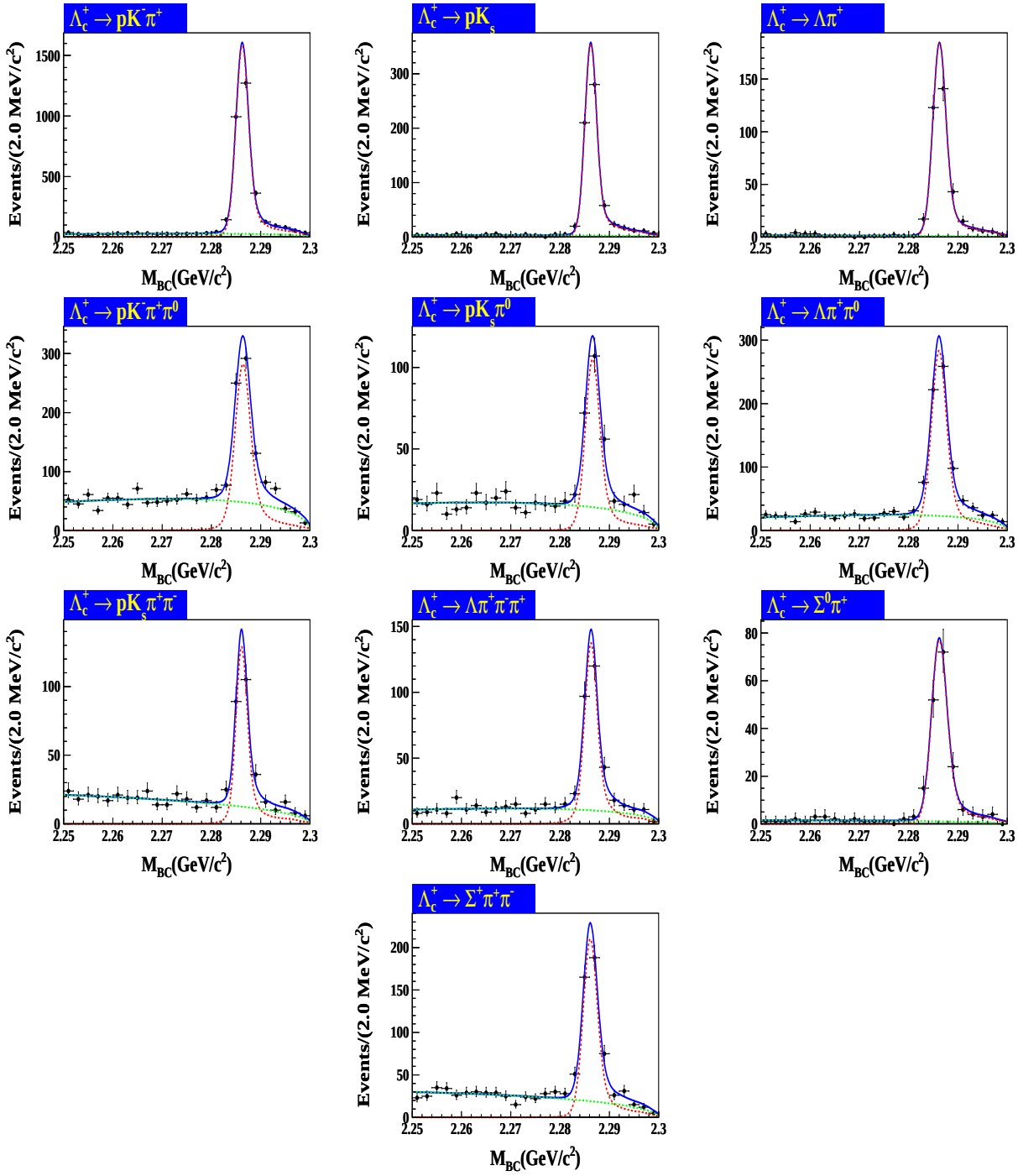

FIG. 11. The fit results of M_{BC} at $\sqrt{s}$ = 4.599 GeV by reconstructing each decay mode of Λ_c^+. The dot with error bar represent data. The blue line is the fitting function. The red histogram is the reconstructed MC shape in MC simulation. The green histogram is the background described with a Argus function which is truncated at 2.3 GeV/c^2.

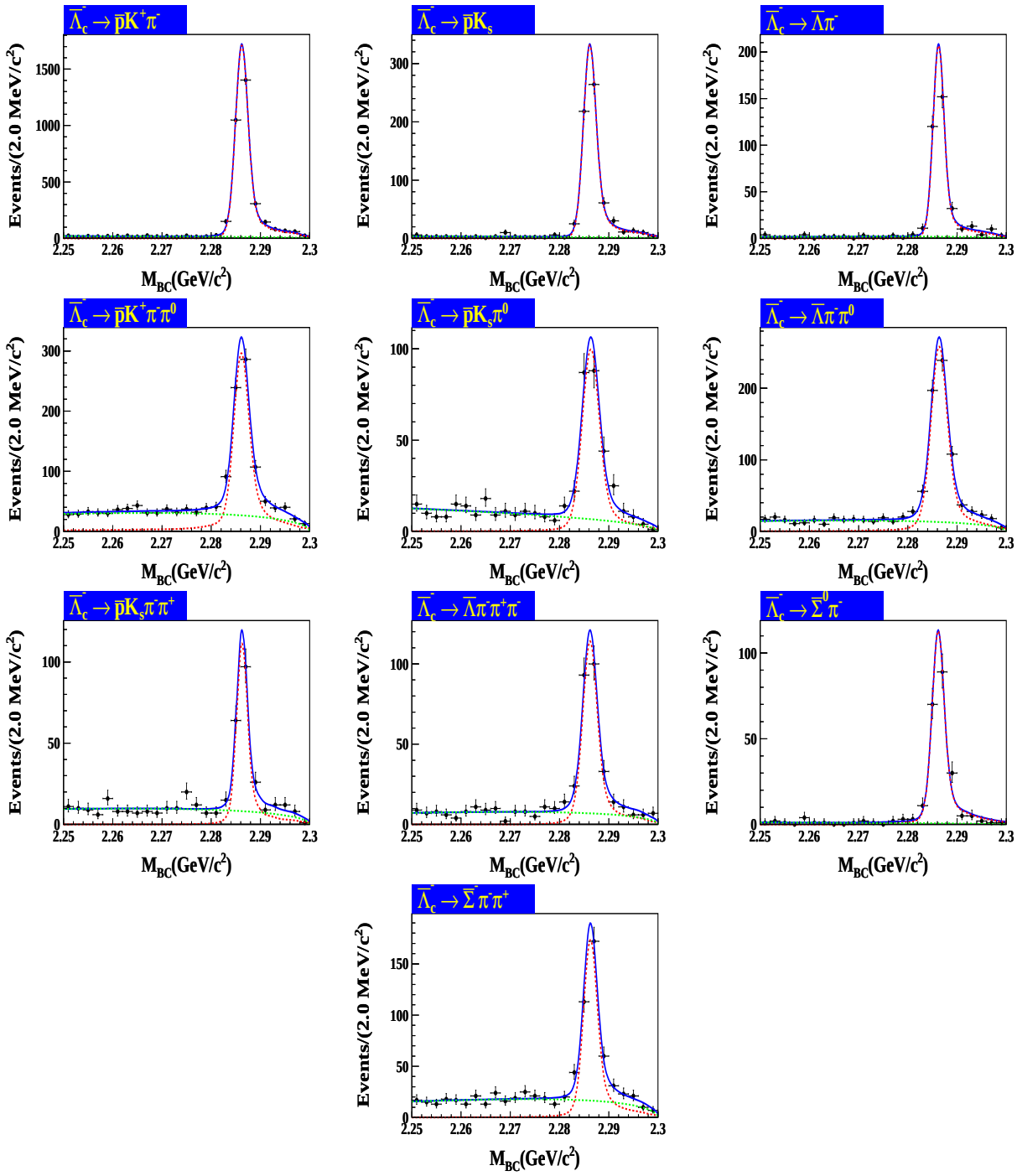

FIG. 12. The fit results of M_{BC} at $\sqrt{s} = 4.599$ GeV by reconstructing each decay mode of $\bar{\Lambda}_c^-$. The dot with error bar represent data. The blue line is the fitting function. The red histogram is the reconstructed MC shape in MC simulation. The green histogram is the background described with a Argus function which is truncated at 2.3 GeV/c^2.

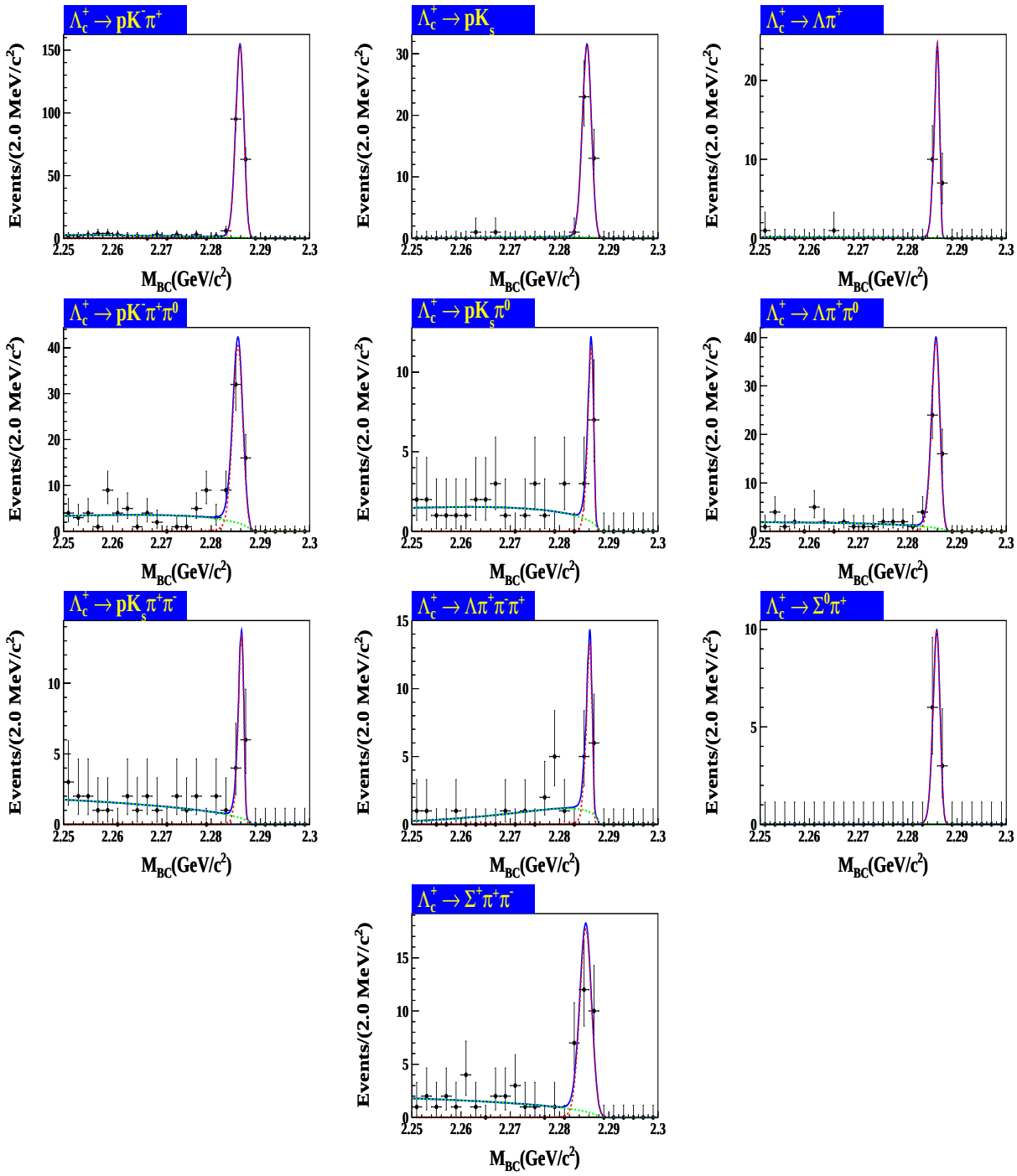

FIG. 13. The fit results of M_{BC} at $\sqrt{s} = 4.574$ GeV by reconstructing each decay mode of Λ_c^+. The dot with error bar represent data. The blue line is the fitting function. The red histogram is the reconstructed MC shape in MC simulation. The green histogram is the background described with a Argus function which is truncated at 2.288 GeV/c^2.

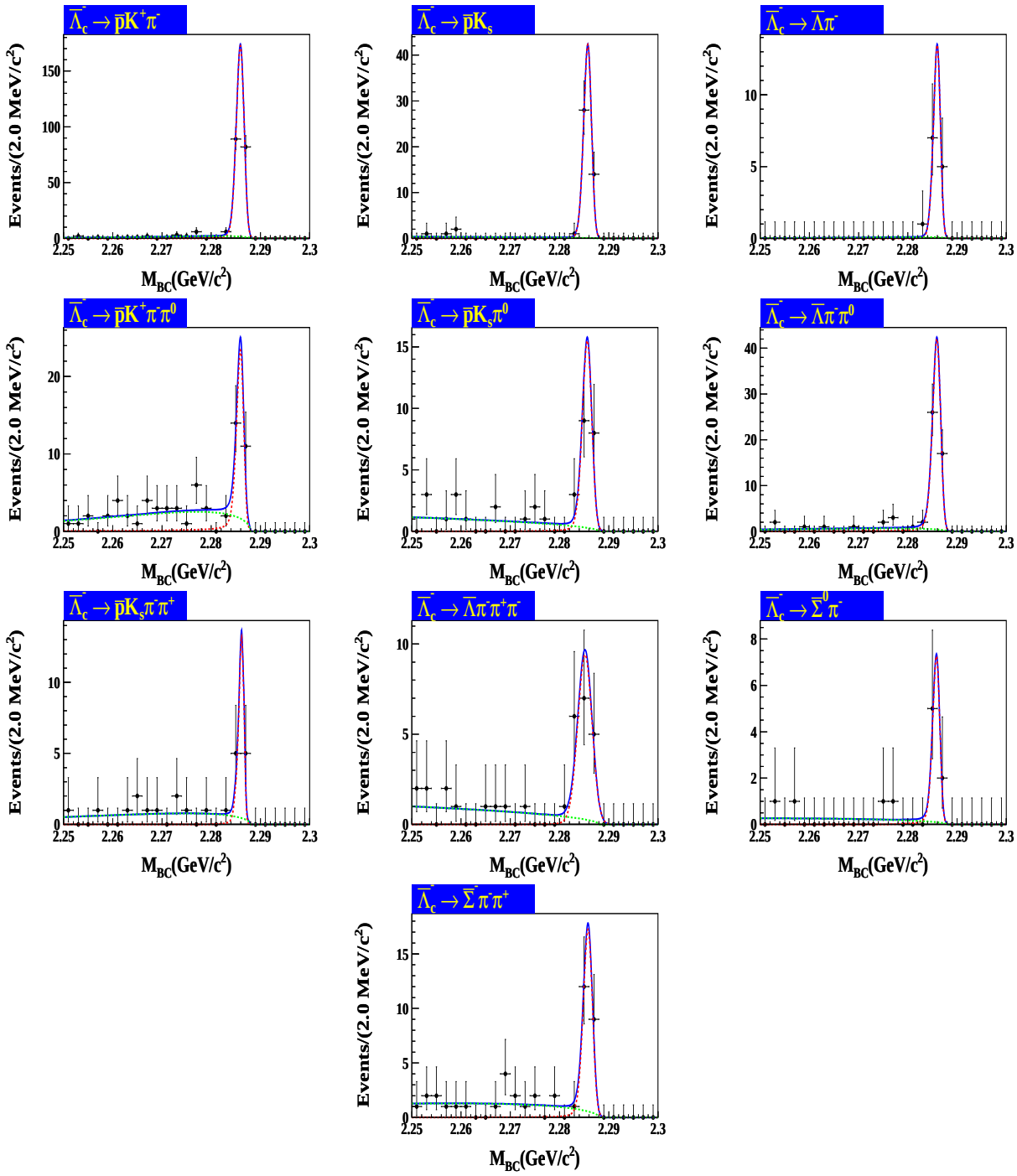

FIG. 14. The fit results of M_{BC} at $\sqrt{s}$ = 4.574 GeV by reconstructing each decay mode of $\bar{\Lambda}_c^-$. The dot with error bar represent data. The blue line is the fitting function. The red histogram is the reconstructed MC shape in MC simulation. The green histogram is the background described with a Argus function which is truncated at 2.288 GeV/c^2.

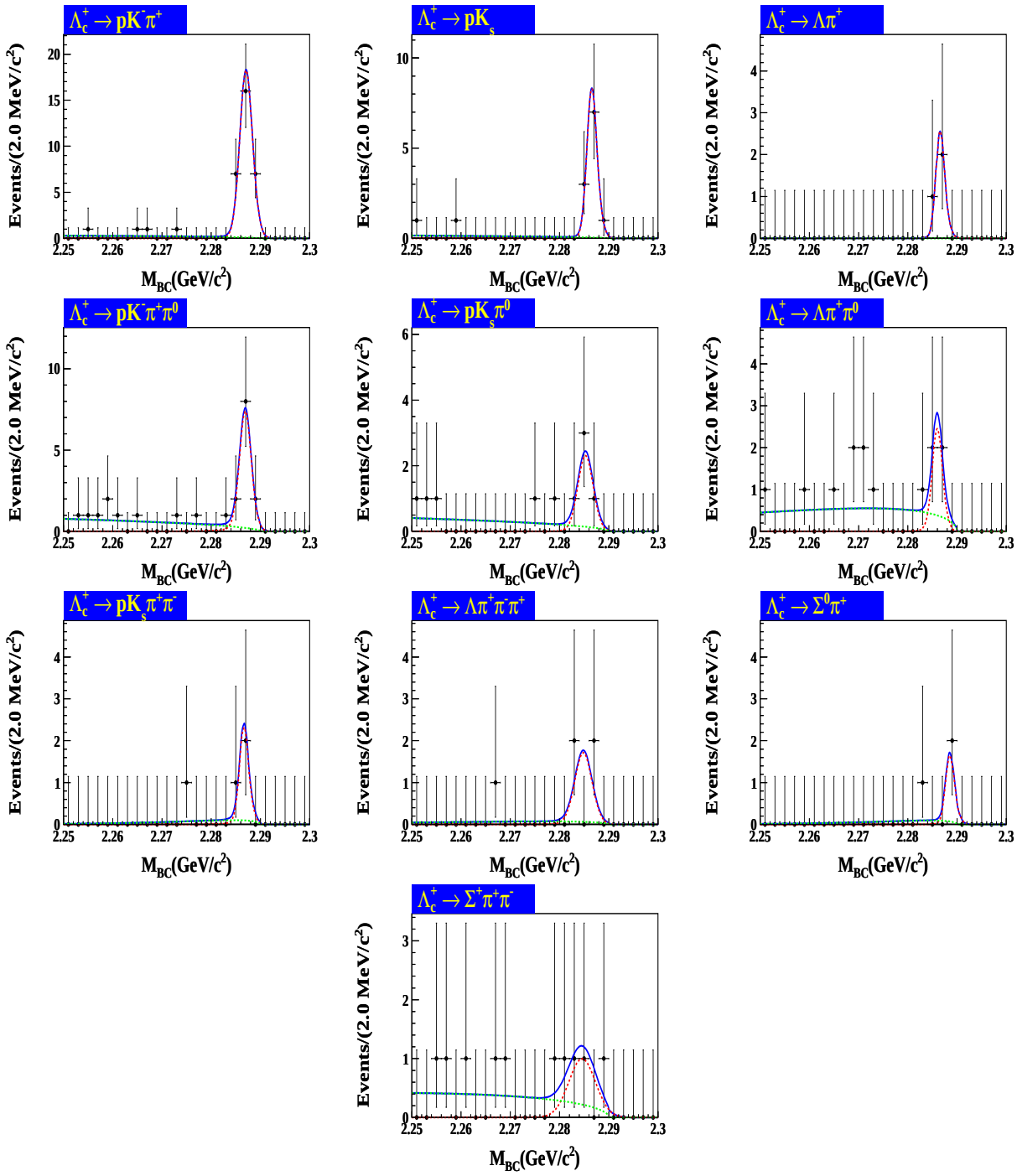

FIG. 15. The fit results of M_{BC} at $\sqrt{s}$ = 4.580 GeV by reconstructing each decay mode of Λ_c^+. The dot with error bar represent data. The blue line is the fitting function. The red histogram is the reconstructed MC shape in MC simulation. The green histogram is the background described with a Argus function which is truncated at 2.290 GeV/c^2.

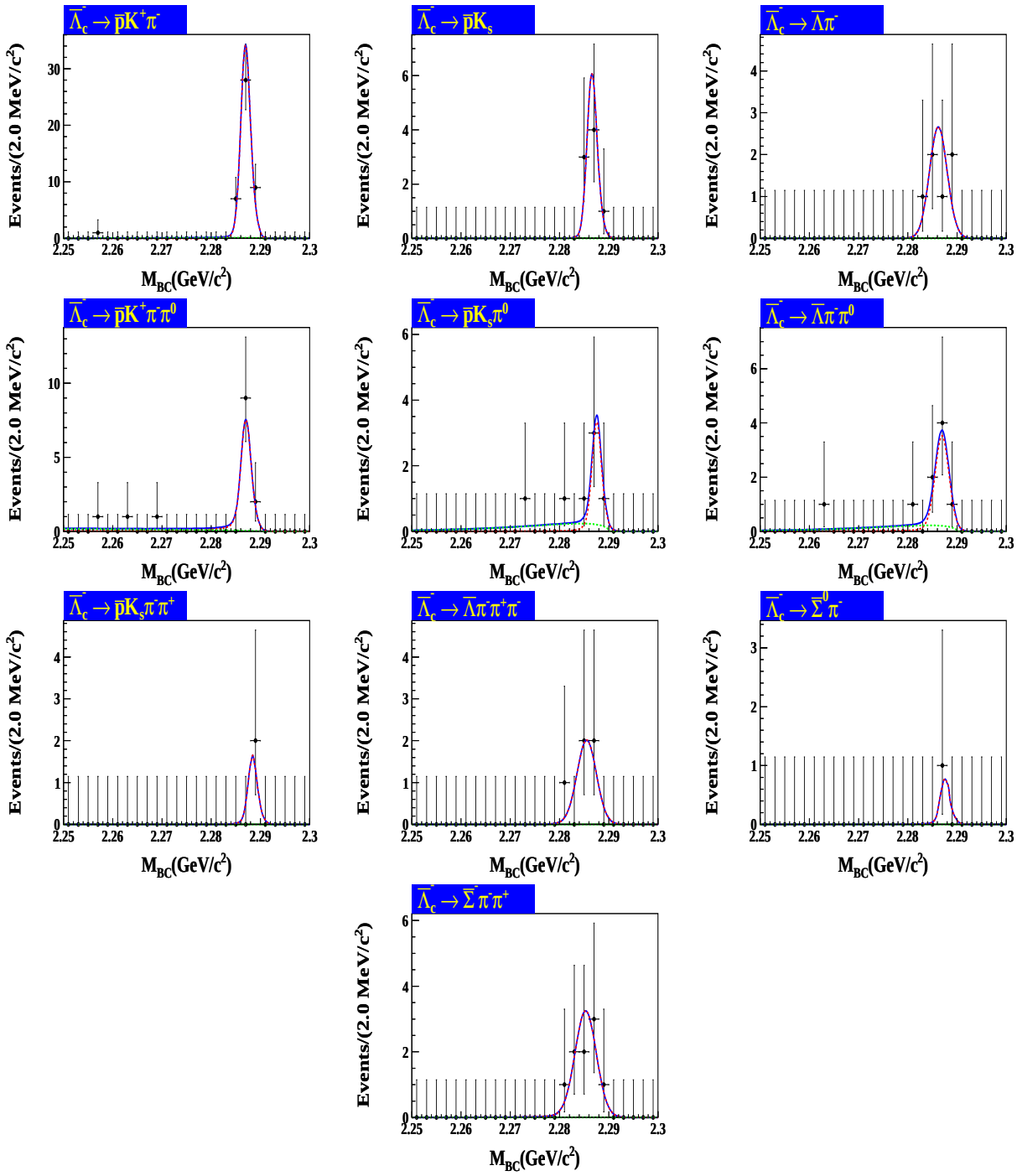

FIG. 16. The fit results of M_{BC} at $\sqrt{s}$ = 4.580 GeV by reconstructing each decay mode of $\bar{\Lambda}_c^-$. The dot with error bar represent data. The blue line is the fitting function. The red histogram is the reconstructed MC shape in MC simulation. The green histogram is the background described with a Argus function which is truncated at 2.290 GeV/c^2.

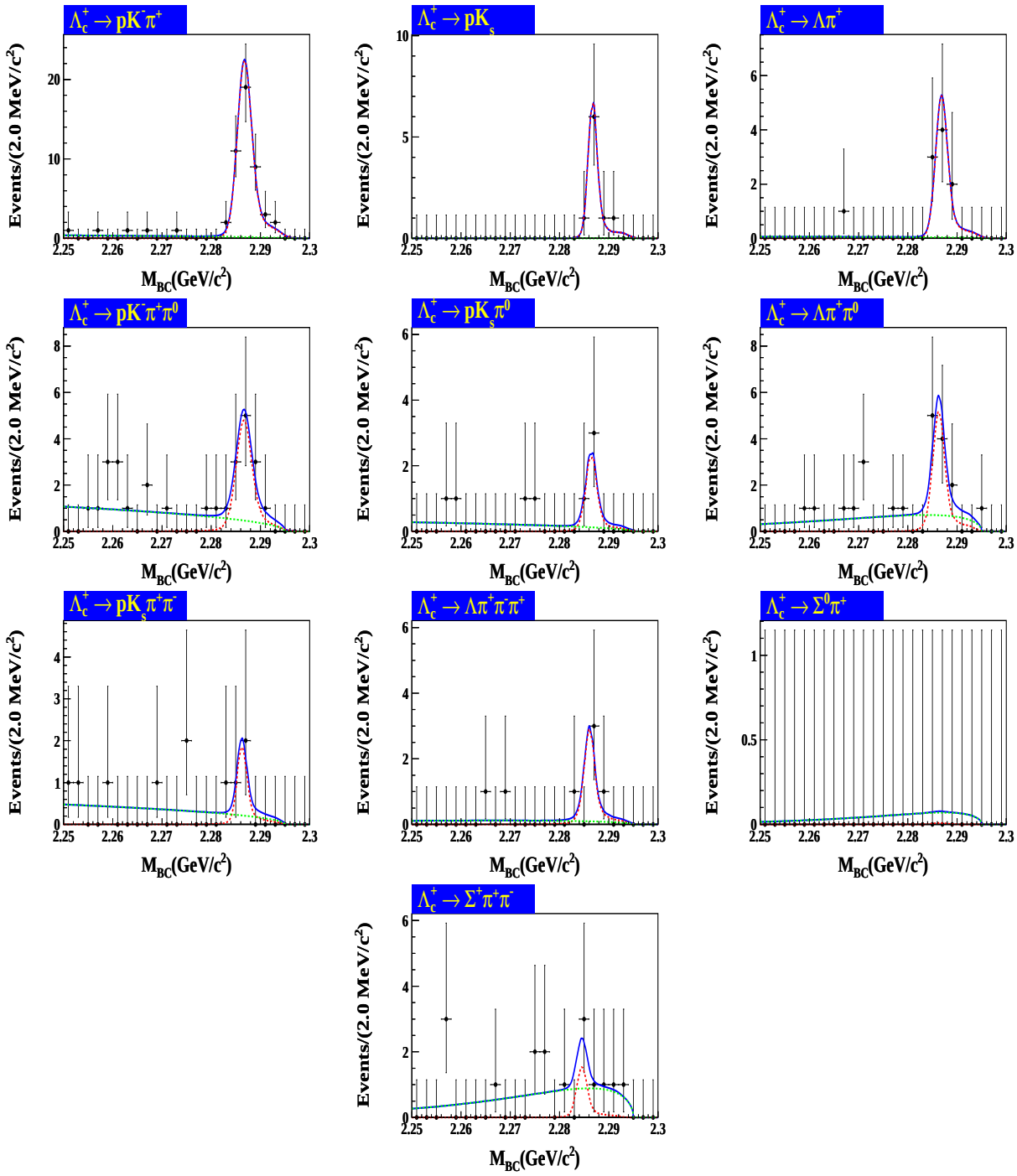

FIG. 17. The fit results of M_{BC} at $\sqrt{s} = 4.590$ GeV by reconstructing each decay mode of Λ_c^+. The dot with error bar represent data. The blue line is the fitting function. The red histogram is the reconstructed MC shape in MC simulation. The green histogram is the background described with a Argus function which is truncated at 2.295 GeV/c^2.

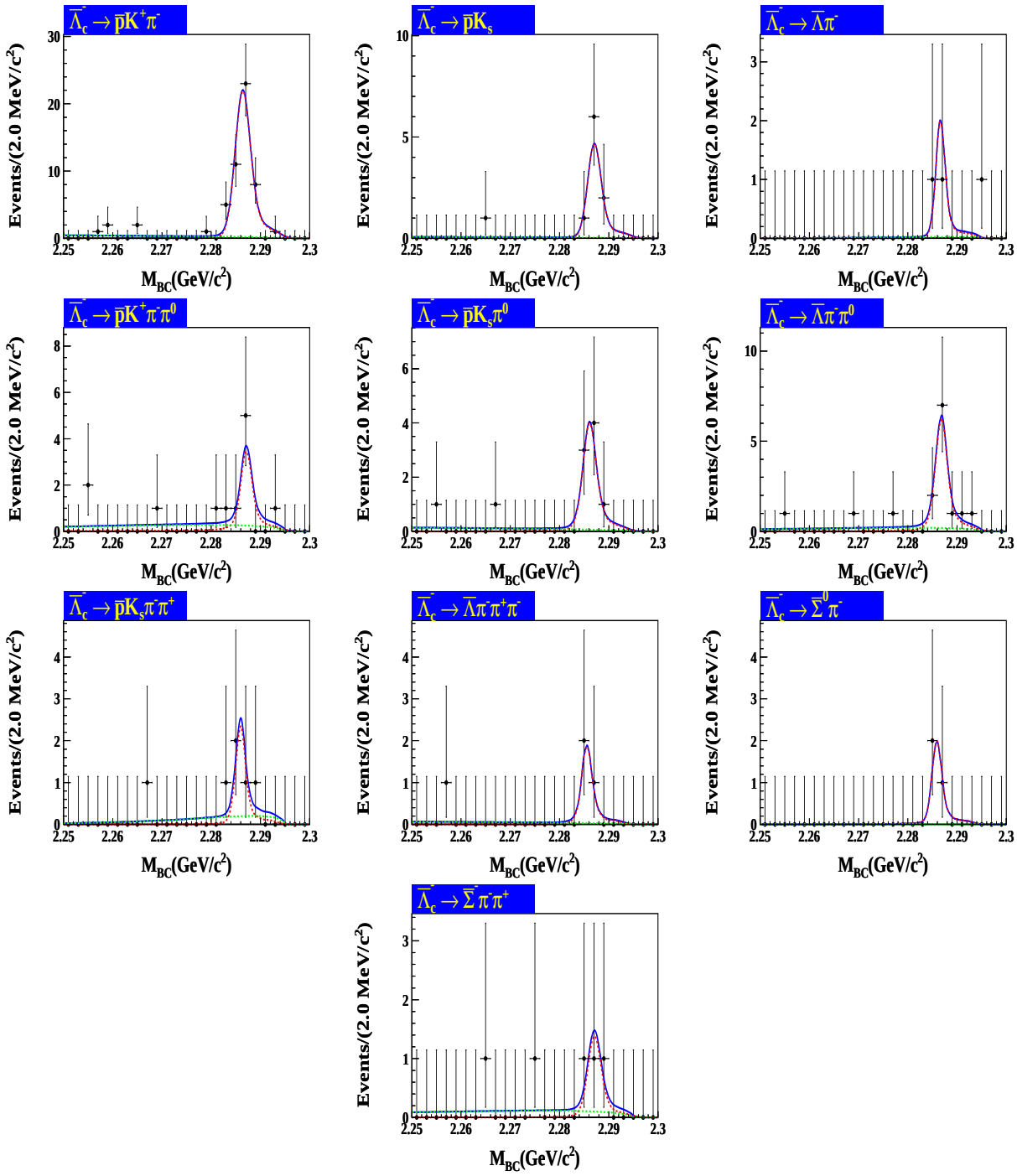

FIG. 18. The fit results of M_{BC} at $\sqrt{s}$ = 4.590 GeV by reconstructing each decay mode of $\bar{\Lambda}_c^-$. The dot with error bar represent data. The blue line is the fitting function. The red histogram is the reconstructed MC shape in MC simulation. The green histogram is the background described with a Argus function which is truncated at 2.295 GeV/c^2.

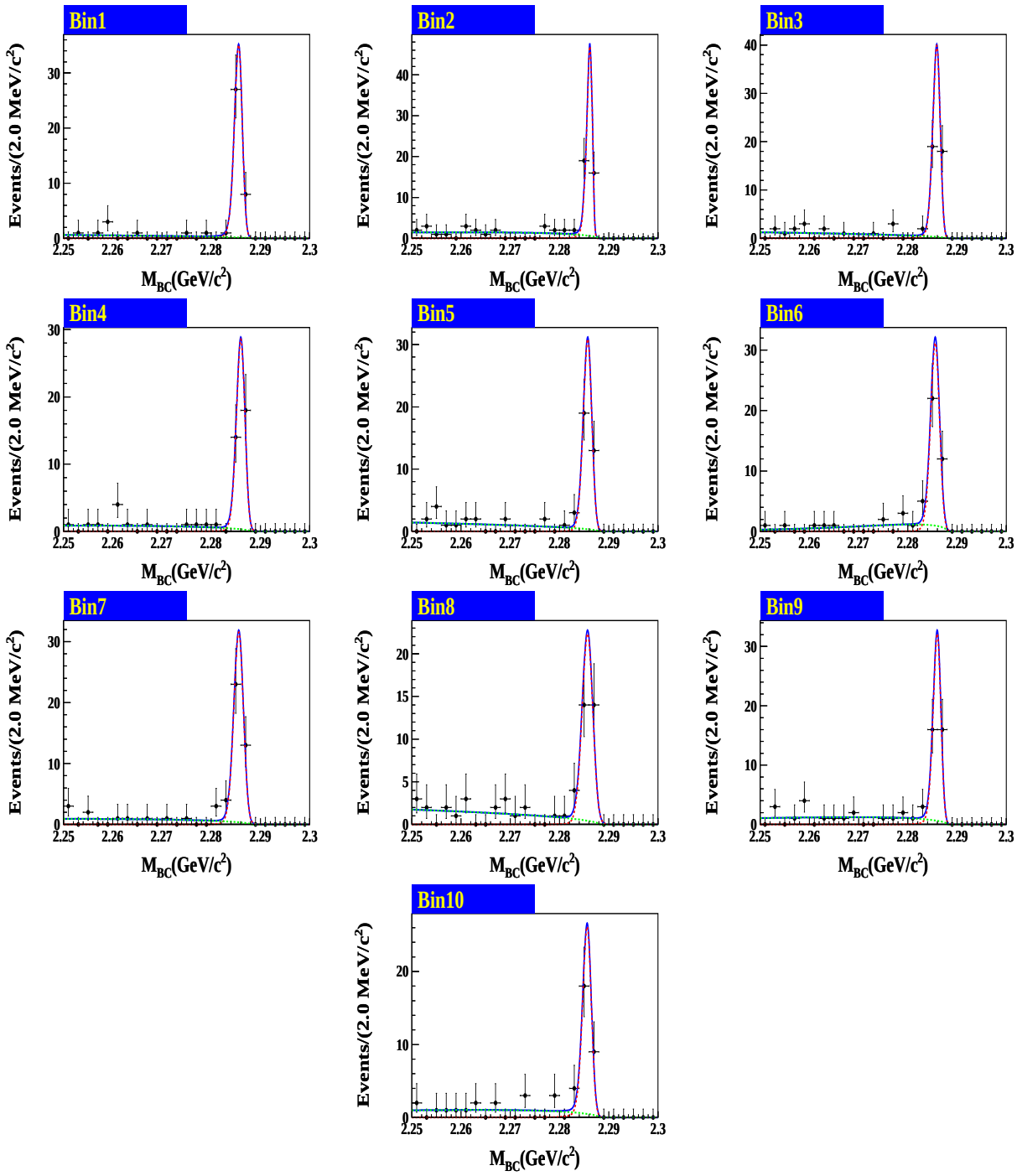

FIG. 19. The fit results of M_{BC} at $\sqrt{s}$ = 4.574 GeV for angular distribution.

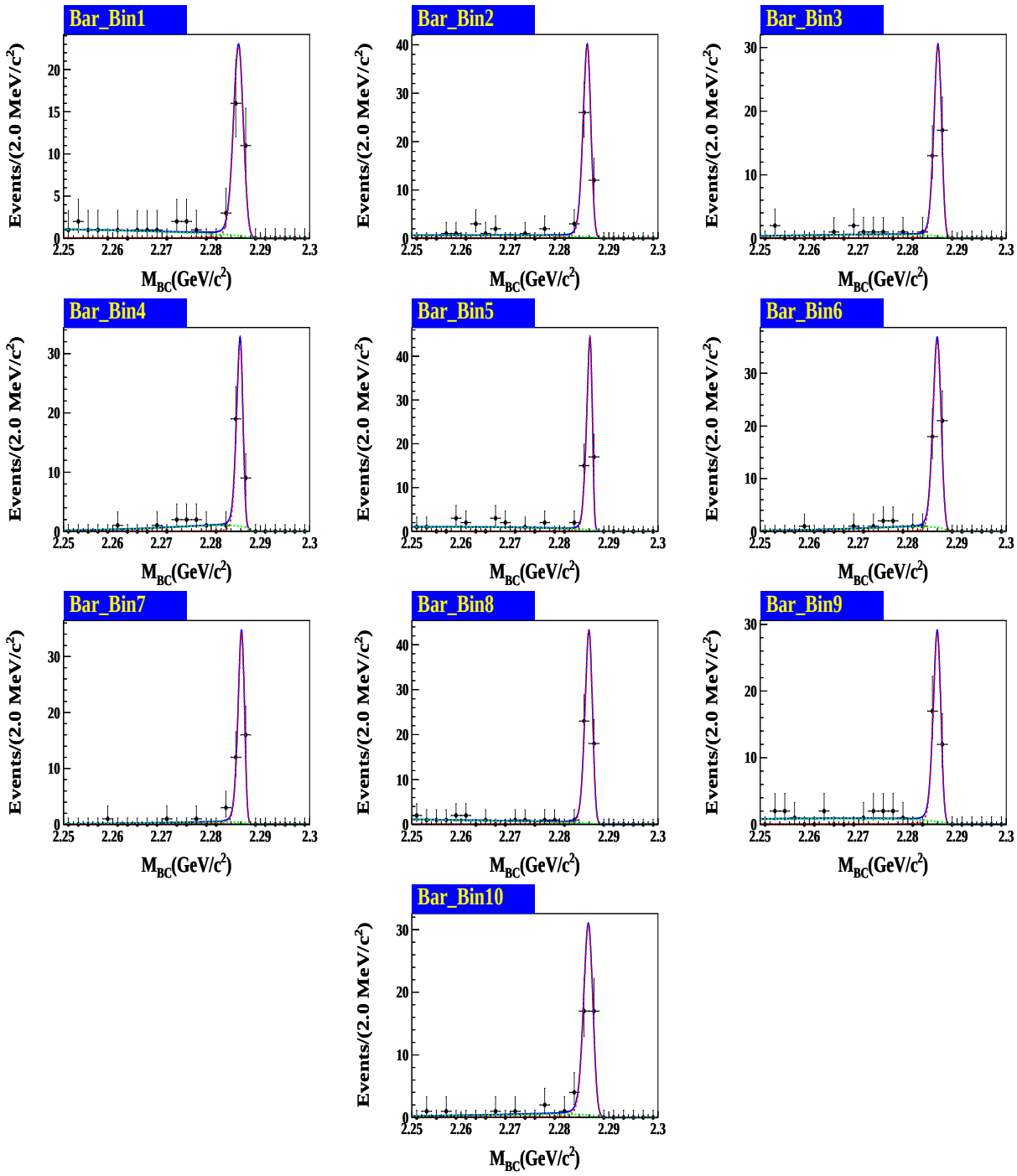

FIG. 20. The fit results of M_{BC} at $\sqrt{s}$ = 4.574 GeV for angular distribution.

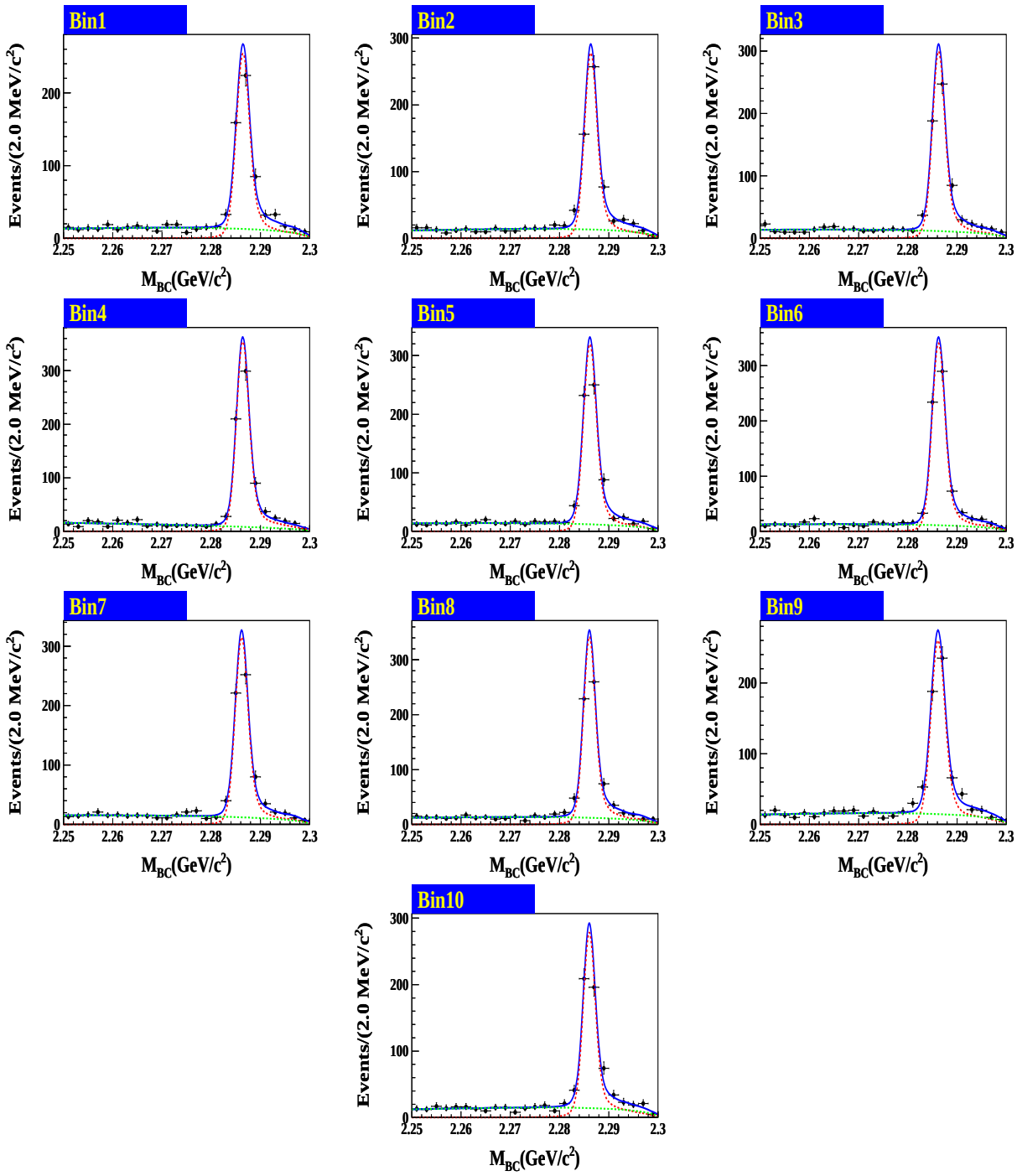

FIG. 21. The fit results of M_{BC} at $\sqrt{s}$ = 4.574 GeV for angular distribution.

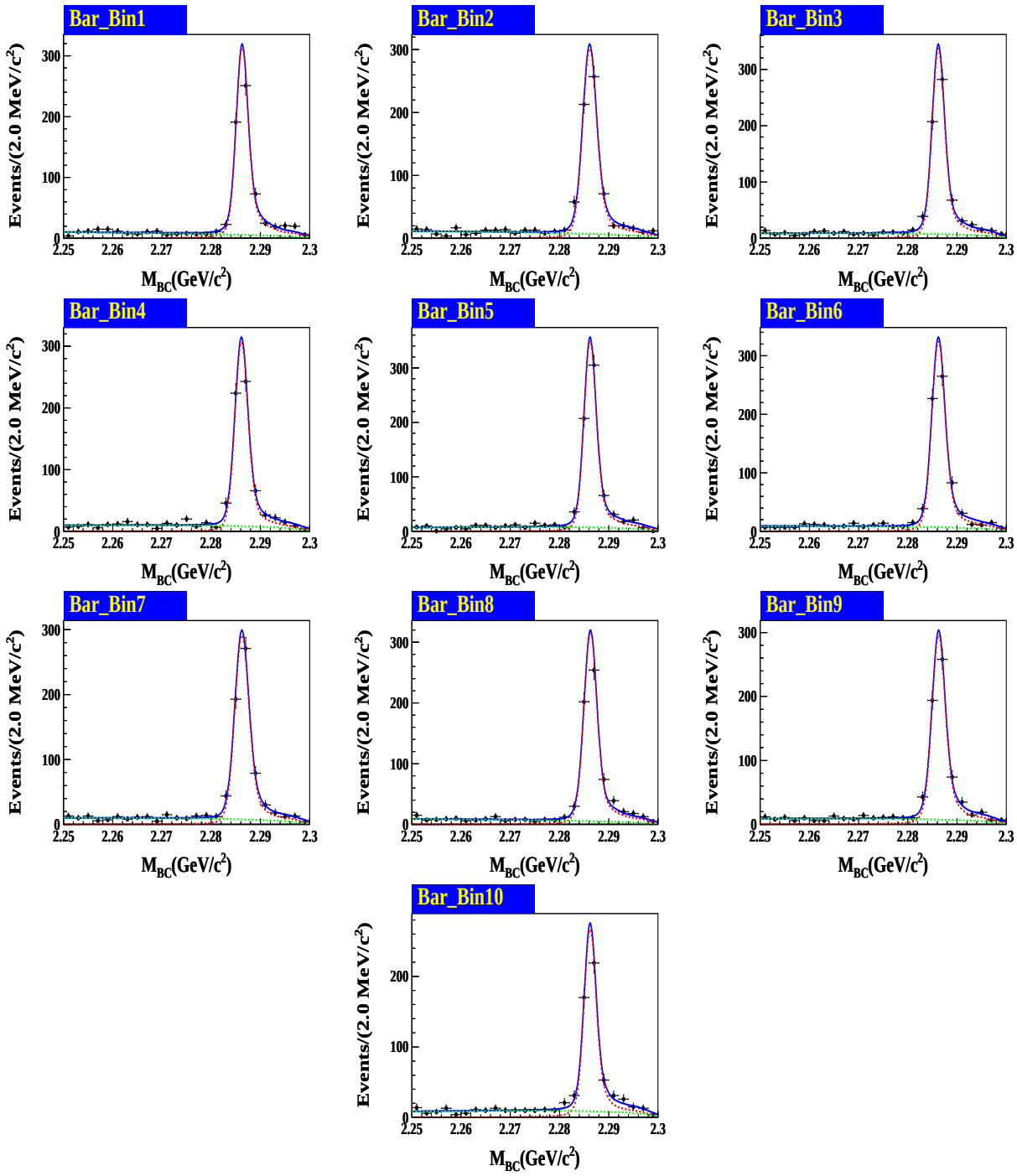

FIG. 22. The fit results of M_{BC} at $\sqrt{s}$ = 4.574 GeV for angular distribution.

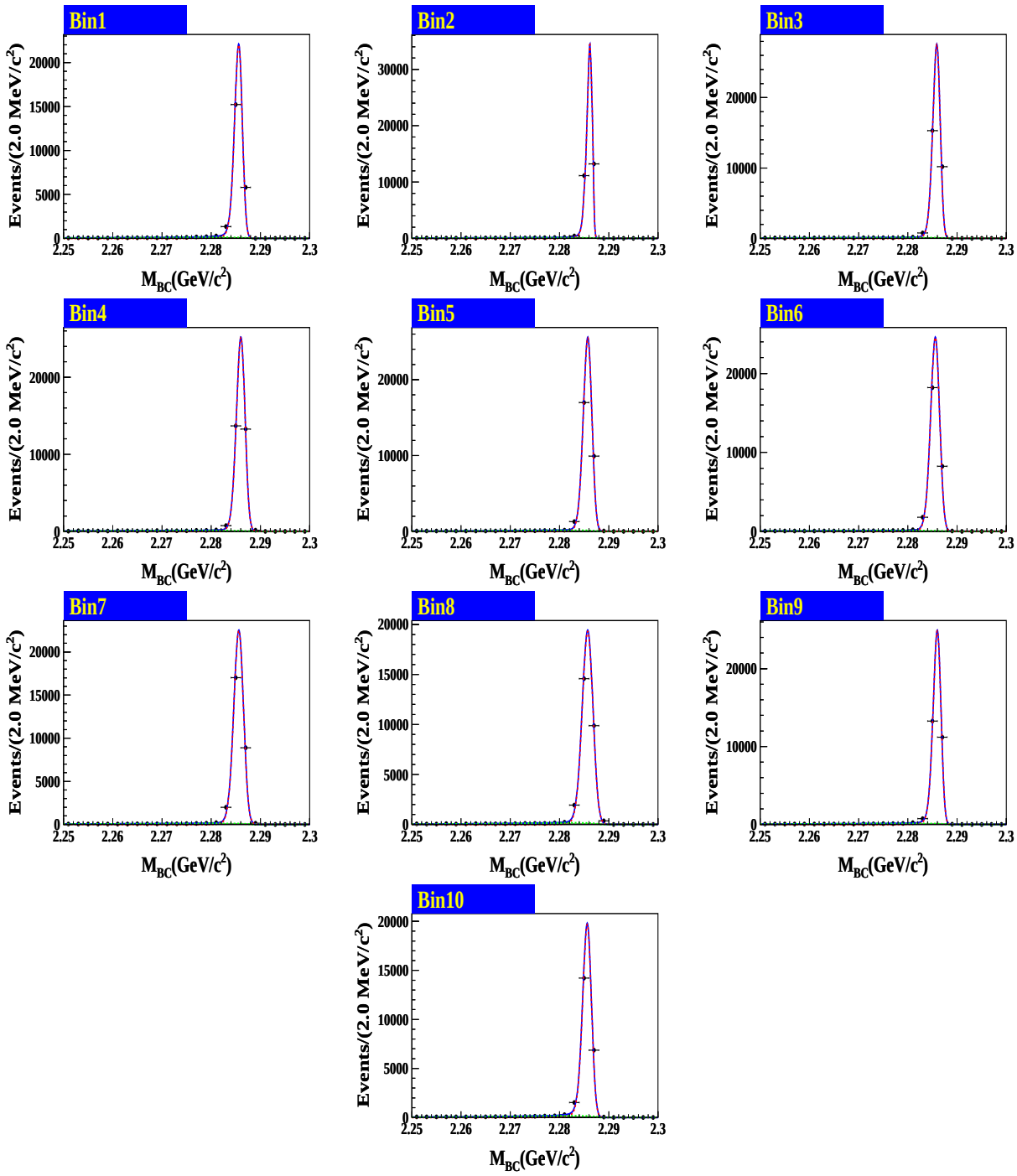

FIG. 23. The fit results of M_{BC} at $\sqrt{s}$ = 4.574 GeV for angular distribution.

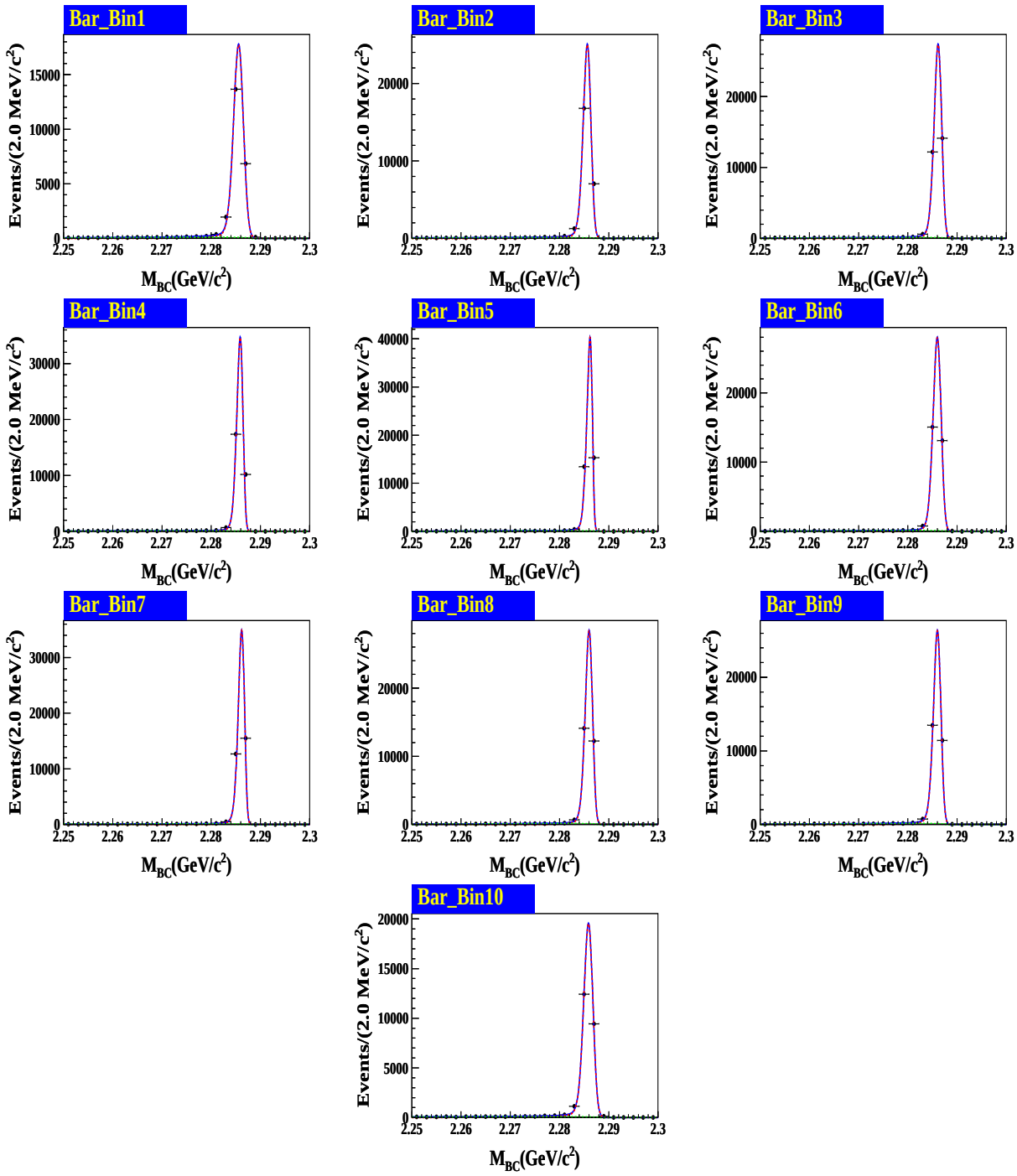

FIG. 24. The fit results of M_{BC} at $\sqrt{s}$ = 4.574 GeV for angular distribution.

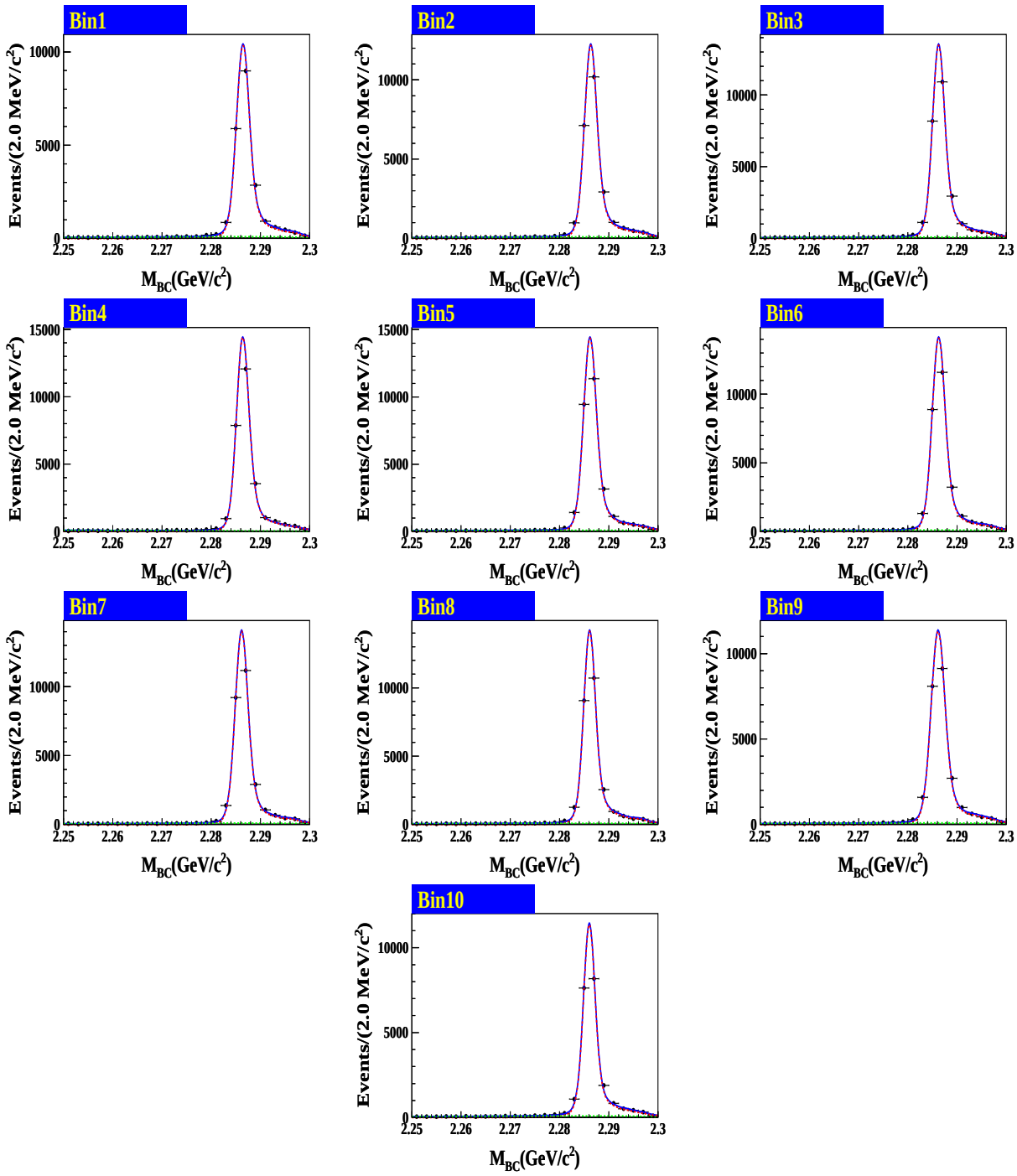

FIG. 25. The fit results of M_{BC} at $\sqrt{s}$ = 4.574 GeV for angular distribution.

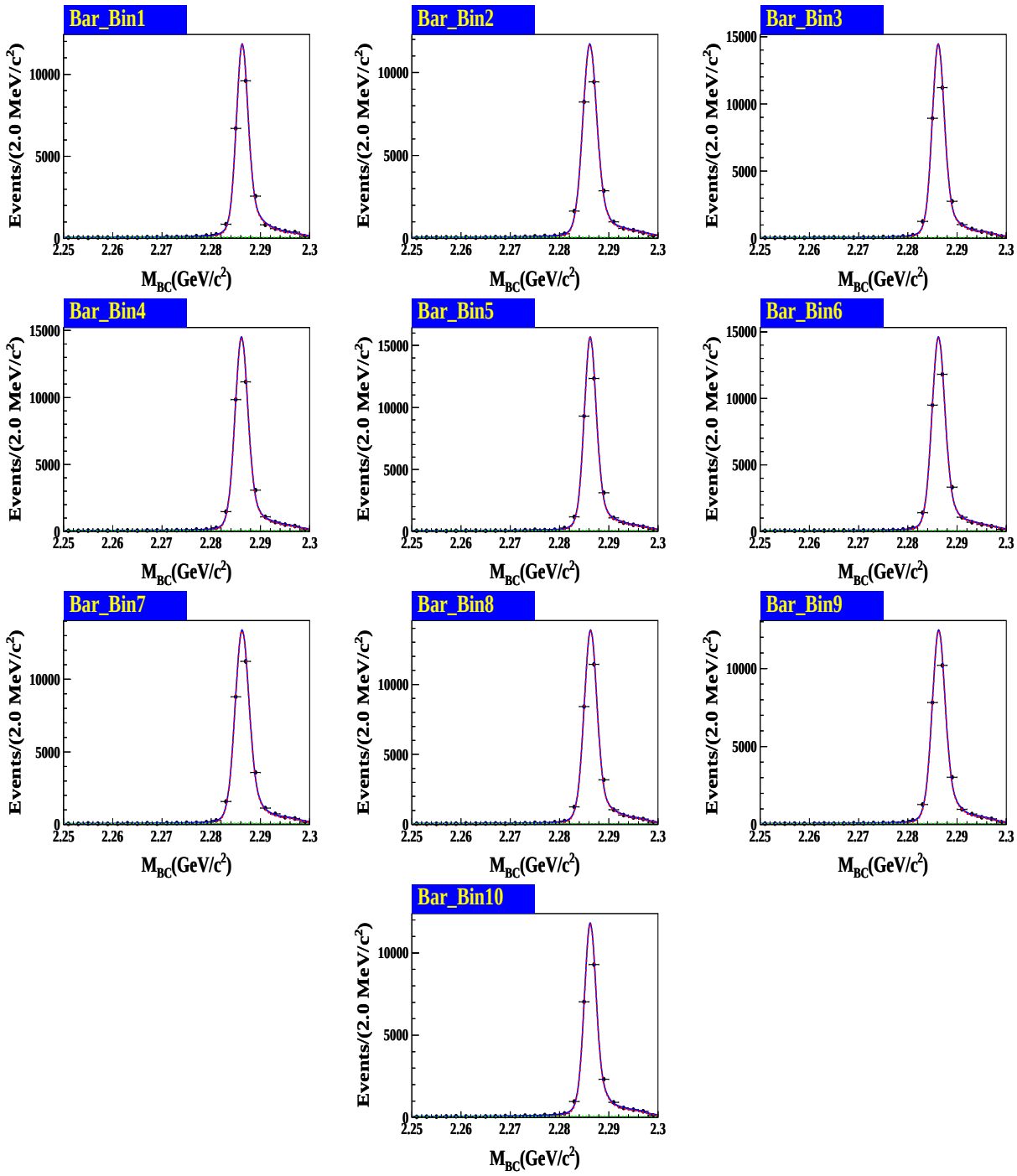

FIG. 26. The fit results of M_{BC} at $\sqrt{s}$ = 4.574 GeV for angular distribution.

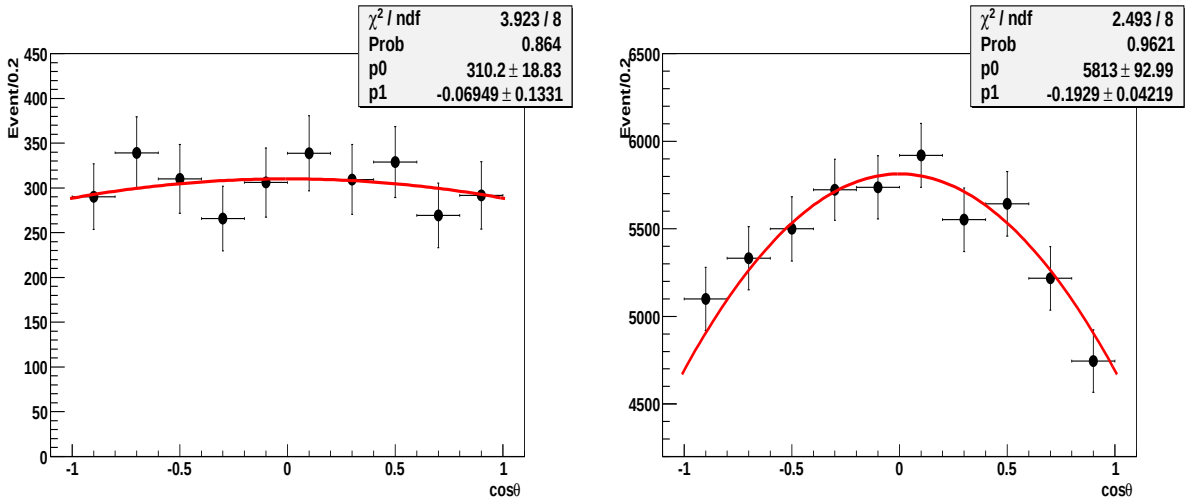

FIG. 27. The angular distribution of 4.574 GeV and 4.599 GeV.

TABLE IV. The calculated cross section for each mode by tagging Λ_c^+ at $\sqrt{s}$ = 4.574.

Mode	$N^{data}_{\Lambda_c^+}$	$\varepsilon_{\Lambda_c^+}$ (%)	BR(%)	$\sigma^{Born}_{\Lambda_c^+}$ (pb)
$pK^-\pi^+$	161.8 ± 12.8	50.9	5.64 ± 0.35	236.1 ± 18.7 ± 17.7
pK^0_S	36.3 ± 6.1	56.2	1.02 ± 0.06	265.1 ± 44.4 ± 16.6
$\Lambda\pi^+$	16.9 ± 4.1	42.8	0.76 ± 0.05	217.7 ± 53.1 ± 16.0
$pK^-\pi^+\pi^0$	52.7 ± 7.9	14.7	4.17 ± 0.36	360.1 ± 53.7 ± 38.4
$pK^0_S\pi^0$	8.6 ± 3.1	17.3	1.20 ± 0.09	172.7 ± 63.4 ± 12.6
$\Lambda\pi^+\pi^0$	42.0 ± 6.7	12.9	4.21 ± 0.25	323.8 ± 51.7 ± 22.1
$pK^0_S\pi^+\pi^-$	9.7 ± 3.2	19.1	1.01 ± 0.09	209.7 ± 69.5 ± 21.5
$\Lambda\pi^+\pi^+\pi^-$	10.0 ± 3.4	10.8	2.34 ± 0.17	166.2 ± 55.9 ± 14.8
$\Sigma^0\pi^+$	9.0 ± 3.0	23.6	0.77 ± 0.05	206.5 ± 68.9 ± 15.1
$\Sigma^+\pi^+\pi^-$	26.4 ± 5.5	17.2	2.06 ± 0.16	312.2 ± 65.3 ± 28.3
summary				241.8 ± 13.8 ± 9.4

TABLE V. The calculated cross section for each mode by tagging $\bar{\Lambda}_c^-$ at $\sqrt{s}$ = 4.574.

Mode	$N^{data}_{\bar{\Lambda}_c^-}$	$\varepsilon_{\bar{\Lambda}_c^-}$ (%)	BR(%)	$\sigma^{Born}_{\bar{\Lambda}_c^-}$ (pb)
$pK^-\pi^+$	172.5 ± 13.5	50.1	5.64 ± 0.35	255.7 ± 20.0 ± 19.1
pK^0_S	42.3 ± 6.5	55.2	1.02 ± 0.06	314.4 ± 48.6 ± 19.7
$\Lambda\pi^+$	12.0 ± 3.5	42.1	0.76 ± 0.05	156.7 ± 45.9 ± 11.5
$pK^-\pi^+\pi^0$	23.1 ± 5.5	15.4	4.17 ± 0.36	150.7 ± 36.1 ± 16.1
$pK^0_S\pi^0$	19.1 ± 4.5	17.2	1.20 ± 0.09	386.6 ± 91.1 ± 28.1
$\Lambda\pi^+\pi^0$	44.7 ± 6.9	13.0	4.21 ± 0.25	342.2 ± 52.8 ± 23.3
$pK^0_S\pi^+\pi^-$	9.4 ± 3.3	18.9	1.01 ± 0.09	206.7 ± 72.2 ± 21.1
$\Lambda\pi^+\pi^+\pi^-$	16.8 ± 4.2	10.4	2.34 ± 0.17	289.0 ± 72.3 ± 25.8
$\Sigma^0\pi^+$	6.9 ± 2.7	24.2	0.77 ± 0.05	155.1 ± 60.0 ± 11.3
$\Sigma^+\pi^+\pi^-$	20.7 ± 4.8	17.3	2.06 ± 0.16	242.8 ± 56.3 ± 22.0
summary				234.9 ± 13.8 ± 9.1

TABLE VI. The calculated cross section for each mode by tagging Λ_c^+ at $\sqrt{s}$ = 4.574.

Mode	$N^{data}_{\Lambda_c^+}$	$\varepsilon_{\Lambda_c^+}$ (%)	BR(%)	$\sigma^{Born}_{\Lambda_c^+}$ (pb)
$pK^-\pi^+$	29.2 ± 5.4	49.3	5.64 ± 0.35	174.4 ± 32.2 ± 13.1
pK^0_S	10.9 ± 3.3	54.0	1.02 ± 0.06	327.4 ± 99.8 ± 20.5
$\Lambda\pi^+$	3.0 ± 1.7	41.3	0.76 ± 0.05	158.7 ± 91.5 ± 11.6
$pK^-\pi^+\pi^0$	11.4 ± 3.5	14.2	4.17 ± 0.36	320.2 ± 98.7 ± 34.1
$pK^0_S\pi^0$	4.5 ± 2.3	16.9	1.20 ± 0.09	369.2 ± 188.3 ± 26.9
$\Lambda\pi^+\pi^0$	3.3 ± 2.2	12.5	4.21 ± 0.25	104.1 ± 68.1 ± 7.1
$pK^0_S\pi^+\pi^-$	2.9 ± 1.7	18.6	1.01 ± 0.09	251.9 ± 153.8 ± 25.8
$\Lambda\pi^+\pi^+\pi^-$	3.8 ± 2.0	10.2	2.34 ± 0.17	262.3 ± 142.6 ± 23.4
$\Sigma^0\pi^+$	1.8 ± 1.3	20.2	0.77 ± 0.05	190.0 ± 140.9 ± 13.9
$\Sigma^+\pi^+\pi^-$	3.3 ± 2.7	16.8	2.06 ± 0.16	158.8 ± 131.0 ± 14.4
summary				188.8 ± 24.1 ± 8.4

TABLE VII. The calculated cross section for each mode by tagging $\bar{\Lambda}_c^-$ at $\sqrt{s}$ = 4.58.

Mode	$N^{data}_{\bar{\Lambda}_c^-}$	$\varepsilon_{\bar{\Lambda}_c^-}$ (%)	BR(%)	$\sigma^{Born}_{\bar{\Lambda}_c^-}$ (pb)
$pK^-\pi^+$	45.0 ± 6.8	49.8	5.64 ± 0.35	259.5 ± 39.1 ± 19.4
pK^0_S	9.0 ± 3.0	53.9	1.02 ± 0.06	264.1 ± 88.1 ± 16.5
$\Lambda\pi^+$	8.9 ± 3.0	40.4	0.76 ± 0.05	467.6 ± 158.3 ± 34.3
$pK^-\pi^+\pi^0$	10.7 ± 3.6	13.9	4.17 ± 0.36	298.9 ± 101.8 ± 31.9
$pK^0_S\pi^0$	3.7 ± 2.0	16.4	1.20 ± 0.09	306.3 ± 165.5 ± 22.3
$\Lambda\pi^+\pi^0$	8.9 ± 3.6	12.4	4.21 ± 0.25	275.4 ± 113.3 ± 18.8
$pK^0_S\pi^+\pi^-$	2.8 ± 1.8	18.5	1.01 ± 0.09	238.5 ± 154.4 ± 24.4
$\Lambda\pi^+\pi^+\pi^-$	4.6 ± 2.3	10.3	2.34 ± 0.17	308.6 ± 153.3 ± 27.5
$\Sigma^0\pi^+$	1.0 ± 9999.0	21.5	0.77 ± 0.05	97.9 ± 978807.3 ± 7.1
$\Sigma^+\pi^+\pi^-$	2.4 ± 2.3	16.9	2.06 ± 0.16	110.3 ± 108.0 ± 10.0
summary				262.3 ± 28.9 ± 11.8

TABLE VIII. The calculated cross section for each mode by tagging Λ_c^+ at $\sqrt{s}$ = 4.59.

Mode	$N^{data}_{\Lambda_c^+}$	$\varepsilon_{\Lambda_c^+}$ (%)	BR(%)	$\sigma^{Born}_{\Lambda_c^+}$ (pb)
$pK^-\pi^+$	46.7 ± 7.0	50.8	5.64 ± 0.35	264.4 ± 39.3 ± 19.8
pK^0_S	8.8 ± 3.0	55.3	1.02 ± 0.06	253.7 ± 85.9 ± 15.9
$\Lambda\pi^+$	2.7 ± 2.1	41.5	0.76 ± 0.05	138.2 ± 108.4 ± 10.1
$pK^-\pi^+\pi^0$	6.2 ± 3.0	15.1	4.17 ± 0.36	160.9 ± 77.0 ± 17.1
$pK^0_S\pi^0$	7.8 ± 2.8	17.1	1.20 ± 0.09	613.6 ± 223.5 ± 44.6
$\Lambda\pi^+\pi^0$	11.1 ± 3.9	13.1	4.21 ± 0.25	325.0 ± 114.6 ± 22.2
$pK^0_S\pi^+\pi^-$	3.4 ± 2.3	18.9	1.01 ± 0.09	292.0 ± 197.0 ± 29.9
$\Lambda\pi^+\pi^+\pi^-$	2.9 ± 1.7	10.4	2.34 ± 0.17	195.8 ± 115.2 ± 17.4
$\Sigma^0\pi^+$	3.0 ± 1.7	22.6	0.77 ± 0.05	277.5 ± 160.2 ± 20.2
$\Sigma^+\pi^+\pi^-$	2.7 ± 1.8	17.5	2.06 ± 0.16	120.5 ± 80.9 ± 10.9
summary				230.4 ± 26.6 ± 10.0

TABLE IX. The calculated cross section for each mode by tagging $\bar{\Lambda}_c^-$ at $\sqrt{s}$ = 4.59.

Mode	$N^{data}_{\bar{\Lambda}_c^-}$	$\varepsilon_{\bar{\Lambda}_c^-}$ (%)	BR(%)	$\sigma^{Born}_{\bar{\Lambda}_c^-}$ (pb)
$pK^-\pi^+$	43.5 ± 6.6	50.9	5.64 ± 0.35	251.3 ± 38.2 ± 18.8
pK^0_S	8.0 ± 2.8	55.6	1.02 ± 0.06	233.3 ± 82.6 ± 14.6
$\Lambda\pi^+$	5.9 ± 2.4	40.8	0.76 ± 0.05	314.9 ± 128.5 ± 23.1
$pK^-\pi^+\pi^0$	10.9 ± 3.3	15.3	4.17 ± 0.36	283.4 ± 86.4 ± 30.2
$pK^0_S\pi^0$	4.2 ± 2.3	17.4	1.20 ± 0.09	338.0 ± 180.5 ± 24.6
$\Lambda\pi^+\pi^0$	6.3 ± 2.8	12.8	4.21 ± 0.25	195.0 ± 87.5 ± 13.3
$pK^0_S\pi^+\pi^-$	1.9 ± 1.3	17.9	1.01 ± 0.09	169.9 ± 120.3 ± 17.4
$\Lambda\pi^+\pi^+\pi^-$	4.9 ± 2.2	10.4	2.34 ± 0.17	337.0 ± 150.8 ± 30.0
$\Sigma^0\pi^+$	1.0 ± 1.0	22.8	0.77 ± 0.05	92.7 ± 92.7 ± 6.8
$\Sigma^+\pi^+\pi^-$	8.8 ± 2.9	17.4	2.06 ± 0.16	406.2 ± 135.3 ± 36.8
summary				241.2 ± 26.2 ± 10.3

TABLE X. The calculated cross section for each mode by tagging Λ_c^+ at $\sqrt{s}$ = 4.599.

Mode	$N^{data}_{\Lambda_c^+}$	$\varepsilon_{\Lambda_c^+}$ (%)	BR(%)	$\sigma^{Born}_{\Lambda_c^+}$ (pb)
$pK^-\pi^+$	2973.8 ± 60.4	51.3	5.64 ± 0.35	231.8 ± 4.7 ± 17.4
pK^0_S	618.8 ± 26.3	55.4	1.02 ± 0.06	247.0 ± 10.5 ± 15.5
$\Lambda\pi^+$	354.4 ± 19.1	41.4	0.76 ± 0.05	254.0 ± 13.7 ± 18.6
$pK^-\pi^+\pi^0$	654.6 ± 35.8	14.4	4.17 ± 0.36	245.9 ± 13.4 ± 26.2
$pK^0_S\pi^0$	224.7 ± 19.8	16.9	1.20 ± 0.09	249.9 ± 22.1 ± 18.2
$\Lambda\pi^+\pi^0$	634.4 ± 32.0	13.0	4.21 ± 0.25	261.4 ± 13.2 ± 17.8
$pK^0_S\pi^+\pi^-$	223.6 ± 19.1	19.5	1.01 ± 0.09	256.1 ± 21.9 ± 26.2
$\Lambda\pi^+\pi^+\pi^-$	270.8 ± 20.2	11.2	2.34 ± 0.17	233.0 ± 17.4 ± 20.8
$\Sigma^0\pi^+$	173.9 ± 14.3	22.3	0.77 ± 0.05	228.4 ± 18.8 ± 16.7
$\Sigma^+\pi^+\pi^-$	443.3 ± 26.4	17.2	2.06 ± 0.16	282.2 ± 16.8 ± 25.6
summary				246.1 ± 4.4 ± 7.9

TABLE XI. The calculated cross section for each mode by tagging $\bar{\Lambda}_c^-$ at $\sqrt{s}$ = 4.599.

Mode	$N^{data}_{\bar{\Lambda}_c^-}$	$\varepsilon_{\bar{\Lambda}_c^-}$ (%)	BR(%)	$\sigma^{Born}_{\bar{\Lambda}_c^-}$ (pb)
$pK^-\pi^+$	3216.0 ± 60.1	49.4	5.64 ± 0.35	260.4 ± 4.9 ± 19.5
pK^0_S	625.0 ± 26.0	53.8	1.02 ± 0.06	256.9 ± 10.7 ± 16.1
$\Lambda\pi^+$	342.0 ± 20.1	40.0	0.76 ± 0.05	253.7 ± 14.9 ± 18.6
$pK^-\pi^+\pi^0$	722.0 ± 36.3	15.1	4.17 ± 0.36	258.6 ± 13.0 ± 27.6
$pK^0_S\pi^0$	250.4 ± 18.5	16.8	1.20 ± 0.09	280.1 ± 20.7 ± 20.4
$\Lambda\pi^+\pi^0$	632.9 ± 31.2	12.5	4.21 ± 0.25	271.2 ± 13.4 ± 18.5
$pK^0_S\pi^+\pi^-$	187.6 ± 18.4	18.8	1.01 ± 0.09	222.8 ± 21.9 ± 22.8
$\Lambda\pi^+\pi^+\pi^-$	251.2 ± 19.4	10.9	2.34 ± 0.17	222.2 ± 17.2 ± 19.8
$\Sigma^0\pi^+$	214.7 ± 14.9	22.2	0.77 ± 0.05	283.3 ± 19.7 ± 20.7
$\Sigma^+\pi^+\pi^-$	366.2 ± 25.0	17.1	2.06 ± 0.16	234.5 ± 16.0 ± 21.2
summary				255.9 ± 4.5 ± 8.2

TABLE XII. The result from tagging the multiple decay modes.

$\sqrt{s}$(GeV)	f_{ISR}	$\sigma^{Born}_{\Lambda_c^+}$ (pb)	$\sigma^{Born}_{\bar{\Lambda}_c^-}$ (pb)
4.574	0.47	242 ± 14 ± 9	235 ± 14 ± 9
4.580	0.67	189 ± 24 ± 8	241 ± 26 ± 10
4.590	0.72	262 ± 29 ± 12	230 ± 27 ± 10
4.599	0.74	246 ± 4 ± 8	256 ± 4 ± 8